

UNBURNED MATERIAL IN THE EJECTA OF TYPE Ia SUPERNOVAE*

GASTÓN FOLATELLI^{1,2}, M. M. PHILLIPS³, NIDIA MORRELL³, MASAOMI TANAKA¹, KEIICHI MAEDA¹, KEN'ICHI NOMOTO¹, MAXIMILIAN STRITZINGER^{4,5}, CHRISTOPHER R. BURNS⁶, MARIO HAMUY², PAOLO MAZZALI^{7,8}, LUIS BOLDT⁹, ABDO CAMPILLAY³, CARLOS CONTRERAS¹⁰, SERGIO GONZÁLEZ³, MIGUEL ROTH³, FRANCISCO SALGADO¹¹, W. L. FREEDMAN⁶, BARRY F MADORE^{6,12}, S. E. PERSSON⁶, AND NICHOLAS B. SUNTZEFF¹³

¹ Institute for the Physics and Mathematics of the Universe (IPMU), University of Tokyo, 5-1-5 Kashiwanoha, Kashiwa, Chiba 277-8583, Japan; gaston.folatelli@ipmu.jp

² Departamento de Astronomía, Universidad de Chile, Casilla 36-D, Santiago, Chile

³ Las Campanas Observatory, Carnegie Observatories, Casilla 601, La Serena, Chile

⁴ The Oskar Klein Centre, Department of Astronomy, Stockholm University, AlbaNova, 10691 Stockholm, Sweden

⁵ Dark Cosmology Centre, Niels Bohr Institute, University of Copenhagen, Juliane Maries Vej 30, 2100 Copenhagen Ø, Denmark

⁶ Observatories of the Carnegie Institution of Washington, 813 Santa Barbara St., Pasadena, CA 91101, USA

⁷ Max-Planck Institut für Astrophysik, Karl-Schwarzschild-Str. 1, 85748 Garching, Germany

⁸ Istituto Naz. di Astrofisica-Oss. Astron., vicolo dell'Osservatorio 5, 35122 Padova, Italy

⁹ Argelander Institut für Astronomie, Universität Bonn, Auf dem Hügel 71, D-53111 Bonn, Germany

¹⁰ Centre for Astrophysics & Supercomputing, Swinburne University of Technology, P.O. Box 218, Victoria 3122, Australia

¹¹ Leiden Observatory, Leiden University, P.O. Box 9513, NL-2300 RA Leiden, The Netherlands

¹² Infrared Processing and Analysis Center, Caltech/Jet Propulsion Laboratory, Pasadena, CA 91125, USA

¹³ George P. and Cynthia Woods Mitchell Institute for Fundamental Physics and Astronomy, Department of Physics and Astronomy, Texas A&M University, College Station, TX 77843, USA

Received 2011 June 20; accepted 2011 October 18; published 2011 December 29

ABSTRACT

The presence of unburned material in the ejecta of normal Type Ia supernovae (SNe Ia) is investigated using early-time spectroscopy obtained by the Carnegie Supernova Project. The tell-tale signature of pristine material from a C+O white dwarf progenitor star is the presence of carbon, as oxygen is also a product of carbon burning. The most prominent carbon lines in optical spectra of SNe Ia are expected to arise from C II. We find that at least 30% of the objects in the sample show an absorption at $\approx 6300 \text{ \AA}$ which is attributed to C II $\lambda 6580$. An alternative identification of this absorption as H α is considered to be unlikely. These findings imply a larger incidence of carbon in SNe Ia ejecta than previously noted. We show how observational biases and physical conditions may hide the presence of weak C II lines, and account for the scarcity of previous carbon detections in the literature. This relatively large frequency of carbon detections has crucial implications on our understanding of the explosive process. Furthermore, the identification of the 6300 \AA absorptions as carbon would imply that unburned material is present at very low expansion velocities, merely $\approx 1000 \text{ km s}^{-1}$ above the bulk of Si II. Based on spectral modeling, it is found that the detections are consistent with a mass of carbon of 10^{-3} to $10^{-2} M_{\odot}$. The presence of this material so deep in the ejecta would imply substantial mixing, which may be related to asymmetries of the flame propagation. Another possible explanation for the carbon absorptions may be the existence of clumps of unburned material along the line of sight. However, the uniformity of the relation between C II and Si II velocities is not consistent with such small-scale asymmetries. The spectroscopic and photometric properties of SNe Ia with and without carbon signatures are compared. A trend toward bluer color and lower luminosity at maximum light is found for objects which show carbon.

Key words: supernovae: general – techniques: spectroscopic

Online-only material: color figures, machine-readable table

1. INTRODUCTION

The generally favored picture of a Type Ia supernova (SN Ia) is the thermonuclear explosion of a C+O white dwarf (WD) star as proposed by Hoyle & Fowler (1960). The WD is assumed to belong to a binary system, and to explode when it reaches the Chandrasekhar mass limit (M_{Ch}) via two main, alternative channels. In the single-degenerate scenario, a main-sequence or giant companion star transfers mass to the WD by Roche-lobe overflow (Whelan & Iben 1973; Nomoto 1982; Iben & Tutukov

1984). Alternatively, in the double-degenerate scenario, the companion star may be another WD, and the M_{Ch} limit is reached or exceeded when both objects coalesce (Iben & Tutukov 1984; Webbink 1984). The actual incidence of each of these evolutionary paths is currently under debate.

Further controversy regarding the physical nature of SNe Ia is related to the mechanism by which the thermonuclear flame propagates inside the WD (see Hillebrandt & Niemeyer 2000, and references therein). It is generally believed that the explosion initiates as a deflagration, i.e., a subsonic flame (Nomoto et al. 1976). If the WD explodes as a prompt detonation, then no intermediate-mass elements would be left in the outer ejecta, as opposed to the observational evidence, and in contradiction with the chemical evolution of the interstellar medium (Arnett et al. 1971). A pure deflagration, however, would not provide the necessary energy and nucleosynthesis to explain most normal

* This paper includes data gathered with the 6.5 m Magellan Telescopes located at Las Campanas Observatory, Chile, and the Gemini Observatory, Cerro Pachon, Chile (Gemini Program GS-2008B–Q–56). This work is based on observations collected at the European Organisation for Astronomical Research in the Southern Hemisphere, Chile (ESO Programmes 076.A-0156, 078.D-0048, 080.A-0516, and 082.A-0526).

SNe Ia (see, e.g., Gamezo et al. 2005). It seems that a delayed detonation, i.e., a transition to a supersonic regime after the WD is pre-expanded in the deflagration phase, is necessary in order to reproduce the typical and bright SNe Ia (Khokhlov 1991; Höflich et al. 1995). The mechanism that produces the transition is not completely understood, mostly due to the complexity of flame-propagation physics and the limited resolution of current models.

Despite these unknowns, SNe Ia are successfully employed as precision cosmological distance indicators due to their homogeneous properties. Their peak luminosities can be calibrated through the observed light-curve width and color to provide distances with a precision of ~ 0.1 mag or better (e.g., see Folatelli et al. 2010, and references therein). This calibrated precision led to the discovery of the acceleration in the current expansion rate of the universe (Riess et al. 1998; Perlmutter et al. 1999).

Some spectral characteristics, such as the strength of Si II lines near maximum light, show variations that are correlated with photometric properties. Temperature in the ejecta has been identified as a possible driver of this luminosity-related spectral diversity (Nugent et al. 1995). Temperature in turn depends on the amount of ^{56}Ni synthesized during the explosion, thus providing a neat physical picture for SNe Ia. However, this one-parameter picture is insufficient to describe inhomogeneities in other photometric and spectroscopic properties that have been observed to vary independently of luminosity. Moreover, the connection of ^{56}Ni mass with temperature produces changes in the opacity which lead to more complex effects in the observed properties (Höflich & Khokhlov 1996; Pinto & Eastman 2000). Kasen & Woosley (2007) performed a detailed study of the line blanketing effects on the light curves and spectra.

The origin of these inhomogeneities has recently been linked to varying properties of the progenitor and explosion mechanism (e.g., see Höflich et al. 2010; Maeda et al. 2011). The latter determines the extent of burning and the degree of mixing of ashes and unburned fuel within the ejecta. During the last decade, multi-dimensional calculations have been introduced in an attempt to fully reproduce the burning process from first principles (see Maeda et al. 2010b, and references therein). These models, although still relatively rudimentary, naturally introduce a variety of effects which may succeed in reproducing several aspects of the observed spectral diversity. For example, an asymmetric explosion, in which the thermonuclear reaction is ignited at an offset from the WD center, provides an explanation not only for the observed scatter of the peak magnitudes (Kasen et al. 2009), but also for the diverse velocity and velocity gradient seen in the Si II $\lambda 6355$ line (Maeda et al. 2010a).

It is an observational fact that spectral inhomogeneities are stronger before or near maximum light than later on (Benetti et al. 2005; Branch et al. 2007). At these early stages the outer part of the ejecta is observed. Under the assumption of homologous expansion (e.g., see Röpke 2005), this outer material moves at high velocities (HVs; $v \gtrsim 10,000$ km s $^{-1}$). As a consequence, observations indicate that, whatever the variations in the progenitor system and explosion mechanism are, the most noticeable effects appear in the fast-expanding, outer regions of the ejecta. Variations are commonly observed among normal SNe Ia in the relative strength of spectral lines, the evolution of expansion velocities, the appearance of HV components, and the presence of different ionization states, among other properties (e.g., see Nugent et al. 1995; Benetti et al. 2005; Mazzali et al. 2005). The study of pre-maximum

spectra thus promises to be very useful in the validation of proposed models.

A relevant characteristic which can be studied using early-time spectra is the possible presence of unburned material in the outer ejecta. Most of the available models predict that part of the primordial WD material composed of carbon and oxygen is left unburned. The amount and location of this unburned material has direct implications on the validity of the models. Since oxygen is also a product of carbon burning, it is the detection of carbon what would most clearly evidence the existence of unburned material. Furthermore, singly ionized states of both C and O are expected to be dominant in the outer ejecta ($v > 10,000$ km s $^{-1}$; Tanaka et al. 2008). Due to high excitation temperatures of O II, however, no strong lines of this ion appear in the optical range. Some strong O I transitions produce observed absorptions which are blended with lines of Mg II, another product of carbon burning. At sufficiently low temperature, C I lines are expected to appear, most prominently in the near-IR (Marion et al. 2006); however, this condition is not likely to occur in the regions of the ejecta probed before maximum light. The same is true for the high-temperature condition required to produce C III lines, unless non-LTE effects play an important role. Consequently, the possible detection of unburned material must rely on the presence of C II lines.

Until recently, the detection of carbon lines in SN Ia spectra was uncommon. C II lines have been clearly identified in optical spectra of a few peculiarly luminous, slowly expanding objects which have been suggested to arise from super-Chandrasekhar mass progenitors (e.g., Howell et al. 2006; Hicken et al. 2007; Yamanaka et al. 2009a; Scalzo et al. 2010). In normal objects, the evidence of carbon is given by a weak absorption feature at ≈ 6300 Å attributed to C II $\lambda 6580$ (Mazzali 2001; Branch et al. 2003; Thomas et al. 2007). An alternative identification of this absorption as H α was suggested by Garavini et al. (2004) for SN 1999aa at 11 days before maximum light. The evidence, however, was not conclusive. Hydrogen from the companion star or a circumstellar envelope could be mixed in the outer layers of the ejecta and possibly be detected in spectra at phases between 15 and 5 days before maximum. Based on spectral synthesis calculations, Lentz et al. (2002) showed that H α can produce the 6300 Å absorption at such early phases if they assumed the existence of $\sim 10^{-2} M_{\odot}$ of hydrogen at $v > 15,000$ km s $^{-1}$. However, such a large amount of hydrogen is in contradiction with the limit of $\sim 10^{-7} M_{\odot}$ imposed by mass-transfer models (Nomoto et al. 2007).

In this paper, we analyze the presence of the C II $\lambda 6580$ line in a sample of pre-maximum spectra obtained by the Carnegie Supernova Project (CSP; Hamuy et al. 2006), and thereby infer the incidence of unburned material in normal SNe Ia. In Section 2, we make a brief description of the spectroscopic data, most of which will be presented by G. Folatelli et al. (2011, in preparation), and provide the evidence supporting the detection of C II lines. The alternative of hydrogen is also studied. In Section 3, we analyze the spectroscopic properties of SNe Ia with carbon in comparison with those which show no clear evidence of it. Section 4 presents a comparative study of photometric properties of SNe with and without carbon. Finally, in Section 5 we briefly discuss our results in light of the available explosion models. Note that between the presentation of a preliminary report on this work (Folatelli 2010) and submission of the current paper, Parrent et al. (2011) published similar results to the ones presented here, confirming a significantly

higher incidence of carbon in SNe Ia spectra than previously noted. In Section 5, we compare the findings of the paper by Parrent et al. (2011) with the conclusions of our own study.

2. DATA SET AND CARBON DETECTION

We base the current work on the sample of optical spectra presented by G. Folatelli et al. (2011, in preparation). This sample consists of 588 spectra of 82 SNe Ia observed by the CSP between 2004 and 2009. In searching for signatures of unburned material, we only consider the pre-maximum phases. This is because any primordial C–O-rich material left by the explosion should lie in the outer parts of the ejecta, and is thus most easily detectable at the earliest stages (Tanaka et al. 2008). For completeness, we have added to the sample of G. Folatelli et al. (2011, in preparation) other spectra in the CSP database which were obtained before maximum light. These additional spectra belong to SNe 2008hj, 2009I, and 2009cz. The present sample amounts to 157 spectra of 51 SNe Ia with ages between -12 and 0 days. Table 1 provides the list of SNe used in this work. The same table also gives the epoch of the first spectrum, the class of carbon detection as defined in Section 2.1, and several photometric parameters which are used in Section 4. Table 2 contains information for each spectrum.

We have also included SN 2009dc which is a luminous, slowly expanding SN Ia suggested to arise from a super-Chandrasekhar mass progenitor (Yamanaka et al. 2009a; Tanaka et al. 2010; Silverman et al. 2011; Taubenberger et al. 2011). For consistency, we only include the pre-maximum spectra of this SN in Table 2, although it showed strong C II features which persisted after maximum light. In light of the peculiar nature of this object, we will treat it in Section 3 as a reference case to see whether there is a connection with the normal SNe Ia studied here.

2.1. The Search for C II

As mentioned in Section 1, carbon is the only element which can be identified with purely unburned material from a C+O WD progenitor. Oxygen instead could be due to a mixture of pristine material and ashes from C burning. According to Tanaka et al. (2008), the dominant carbon ionization state in the outer parts of the ejecta is C II. Therefore, in our study of pre-maximum spectra, we search for signatures of unburned material in the form of C II features.

The four strongest C II lines at optical wavelengths are C II $\lambda 4267$, $\lambda 4745$, $\lambda 6580$, and $\lambda 7234$. Of these, the most prominent in SN Ia spectra is expected to be C II $\lambda 6580$ (e.g., see Hatano et al. 1999; Mazzali 2001). Even if C II $\lambda 4745$ has a lower oscillator strength than C II $\lambda 6580$, it may become comparably strong at temperatures of ≈ 5000 K due to its lower excitation energy. However, at such low temperatures, the blue part of the spectrum is dominated by Ti II lines, which complicates the identification of this carbon feature. For expansion velocities between $10,000$ and $20,000$ km s^{-1} the C II $\lambda 6580$ line should produce absorption between 6170 Å and 6370 Å, which lies on the red side of the Si II $\lambda 6355$ line. We have therefore focused the search for unburned material in this wavelength region.

Visual inspection of the spectra allowed us to divide the present SN sample into three main groups. First, those SNe which show no apparent absorption but rather a clear emission component of the Si II $\lambda 6355$ line. They are marked with “N” (i.e., “no detection”) in Table 1. Objects that do show a clear absorption feature, usually centered at ≈ 6320 Å are indicated

with an “A” (i.e., “absorption”) in Table 1. An intermediate case is that of SNe which show no clear absorption but an apparently suppressed Si II $\lambda 6355$ emission component. Because of the flat emission profile, these are labeled “F” (i.e., “flat emission”) in Table 1. We note that the distinction between groups A and F is not a quantitative one, and the specific classification may depend in each case on the quality of the available data. Nevertheless, this does not affect the results of the forthcoming analysis. Finally, for those cases which are inconclusive—typically due to data with low signal-to-noise ratio—we have added a “?” to the identification. In the cases of SNe 2007S, 2008ar, 2008gp, and 2009ad, the available spectra do not cover the wavelength range under scrutiny and thus we are not able to classify them according to the presence of the putative C II $\lambda 6580$ line. Figure 1 shows the spectra which belong to group A in the wavelength regions of the four C II lines. Figure 2 shows the spectra with flat Si II $\lambda 6355$ emission. In the left panel we include SNe in the F group while in the right panel objects are classified as “F?.” As a comparison, several “non-detections,” i.e., SNe in group N, are shown in Figure 3.

We have subsequently studied the spectral regions corresponding to the other three C II lines in search of similar features which may help consolidate the identification with this ion. Although in the case of some A-type objects other absorptions at the right locations can be seen (Figure 1), these are usually very weak and it is difficult to clearly associate them with C II. In particular, the two lines on the blue part of the spectrum are subject to severe blending into stronger lines, mainly of Mg II, Si II, S II, and Fe II. Moreover, an absorption matching the expected position of the C II $\lambda 4745$ line is seen in most of the spectra, irrespective of the SN belonging to the A, F, or N types. The absorption due to C II $\lambda 7234$, depending on the redshift and expansion velocity, may lie near the 6900 Å telluric band, which may affect the detection if the atmospheric feature is not accurately removed.

A more careful identification of spectral lines can be carried out using the highly parameterized SN synthetic spectrum code SYNOW (see Branch et al. 2002, and references therein). Examples of synthetic spectra compared with observations are shown in Figures 4–7. Due to the approximations involved in SYNOW (spherical symmetry, sharp photosphere, LTE, Sobolev line formation, etc.), the synthetic spectra are not expected to produce a perfect match to the observed flux and line profiles. Nevertheless, SYNOW is useful for identifying spectral features with the species which produce them, specifically by reproducing the location of observed absorptions with predicted lines of a given ion.

Table 3 provides a summary of the main parameters used to produce the synthetic spectra shown in Figures 4–7. In order to simplify the analysis, several other parameters have been left fixed. In particular, we have adopted a power law of index 8 for the dependence of the optical depth on velocity, up to $30,000$ km s^{-1} . We have also fixed the excitation temperature to $T_{\text{exc}} = 12,000$ K for all species.

Figures 4 and 5 show the cases of two objects in group A, namely, SNe 2005el and 2009F at -7 and -5 days, respectively. These SNe show different $\Delta m_{15}(B)$ values and correspondingly distinct spectroscopic properties. While SN 2005el is a normal event, SN 2009F presents fast-declining light curves and belongs to the “Cool” or “CL” type in the scheme of Branch et al. (2006). The latter SN shows a relatively red spectrum and strong absorptions due to Ti II and O I, as compared with normal SNe Ia. The synthetic spectra provide satisfactory matches to the

Table 1
Sample of SNe Ia

SN	First Epoch	C II Class	m_B (mag)	$(B - V)_{\max}$ (mag)	$\Delta m_{15}(B)$ (mag)	$E(B - V)_{\text{host}}$ (mag)	Low Reddening	z_{Helio}	M_B (mag)	ΔM_B (mag)
(1)	(2)	(3)	(4)	(5)	(6)	(7)	(8)	(9)	(10)	(11)
2004dt	-8.7	N	15.000(035)	-0.046(047)	1.24(07)	-0.046(068)	...	0.01973	-19.51(12)	-0.39(18)
2004ef	-8.5	N	16.828(019)	0.102(027)	1.38(06)	0.085(057)	...	0.03099	-18.69(08)	-0.09(12)
2004eo	-11.1	N	15.067(011)	0.055(020)	1.36(06)	0.039(054)	Y	0.01570	-18.90(15)	-0.16(17)
2004ey	-0.8	N	14.713(011)	-0.063(022)	0.93(01)	-0.027(055)	...	0.01579	-19.24(15)	0.15(16)
2004gs	-3.3	N	17.132(017)	0.158(044)	1.61(08)	0.02665	-18.21(08)	0.07(16)
2004gu	-2.9	N	17.478(017)	0.189(021)	0.89(30)	0.231(054)	...	0.04586	-19.05(05)	-0.33(23)
2005M	-0.1	N	15.924(038)	0.018(039)	0.84(07)	0.065(063)	...	0.02201	-19.02(10)	0.21(16)
2005ag	0.3	N	18.447(060)	-0.003(125)	0.92(17)	0.035(135)	...	0.07943	-19.30(07)	-0.07(37)
2005bl	-8.4	F?	18.221(031)	0.558(035)	1.80(04)	0.02406	-16.92(09)	0.12(14)
2005bo	-1.0	N	15.662(009)	0.290(017)	1.30(08)	0.282(053)	...	0.01390	-18.34(15)	-0.19(16)
2005el	-7.3	A	14.821(021)	-0.014(022)	1.35(04)	-0.028(055)	Y	0.01491	-19.17(15)	-0.22(16)
2005eq	-5.2	N	16.306(026)	0.099(042)	0.77(02)	0.155(065)	...	0.02898	-19.11(08)	-0.05(14)
2005hc	-5.2	N	17.305(033)	0.004(036)	0.91(09)	0.043(062)	Y	0.04594	-19.14(06)	0.08(13)
2005ke	-1.4	N	14.772(021)	0.661(023)	1.76(05)	0.00488	-17.07(08)	-0.28(11)
2005ki	-7.6	N	15.543(031)	-0.008(031)	1.37(05)	-0.025(059)	Y	0.01921	-19.13(11)	-0.22(15)
2006D	-6.1	A	14.136(006)	0.094(013)	1.39(01)	0.075(052)	Y	0.00853
2006X	-10.4	N	15.218(048)	1.196(058)	1.11(03)	1.210(077)	...	0.00524	-15.69(15)	0.11(22)
2006ax	-10.5	F	15.002(028)	-0.048(028)	1.02(02)	-0.022(057)	Y	0.01674	-19.40(13)	-0.11(15)
2006dd	-10.8	A	12.241(009)	-0.071(013)	1.08(01)	-0.053(052)	Y	0.00587	-19.01(05)	0.29(06)
2006gt	-0.3	N	18.229(020)	0.256(024)	1.85(29)	0.04477	-18.15(06)	-0.31(23)
2006hx	-9.6	N	17.510(031)	-0.157(073)	1.15(04)	-0.147(088)	...	0.04549	-18.90(06)	0.58(21)
2006kf	-5.1	N	15.817(005)	-0.016(033)	1.58(04)	-0.058(060)	Y	0.02130	-18.91(11)	-0.13(14)
2006mr	-2.3	N	15.345(011)	0.708(121)	1.78(04)	0.00587	-15.90(05)	0.75(34)
2006os	-1.9	N	17.500(020)	0.314(024)	1.44(07)	0.289(055)	...	0.03281	-18.19(07)	-0.21(11)
2007A	-6.2	F	15.695(012)	0.222(033)	0.92(02)	0.259(060)	...	0.01765	-18.52(13)	0.09(16)
2007S	-11.9	...	15.789(013)	0.371(031)	0.95(03)	0.405(059)	...	0.01388	-18.22(15)	-0.03(17)
2007af	-11.1	A	13.330(014)	0.196(030)	1.20(03)	0.200(059)	...	0.00546
2007ai	-2.7	N	16.805(009)	0.119(011)	0.74(01)	0.178(051)	...	0.03166	-18.87(07)	0.16(08)
2007as	-2.2	N	15.387(006)	0.052(008)	1.22(01)	0.054(051)	...	0.01757	-19.01(12)	-0.14(12)
2007ax	-2.1	N	16.201(029)	0.684(031)	1.96(09)	0.00686
2007bd	-7.5	N	16.551(022)	0.029(024)	1.23(06)	0.029(056)	...	0.03102	-19.12(07)	-0.21(11)
2007jg	-0.2	N	17.181(045)	0.028(048)	1.31(08)	0.019(070)	...	0.03713	-18.80(08)	0.06(16)
2007le	-9.2	F?	13.875(009)	0.292(011)	0.97(07)	0.323(051)	...	0.00672
2007on	-3.9	F?	13.023(008)	0.088(011)	1.86(03)	...	Y	0.00649
2008ar	-8.1	...	16.259(038)	0.100(054)	0.88(07)	0.142(073)	...	0.02615	-19.06(09)	-0.09(18)
2008bc	-10.1	N	14.624(007)	-0.038(015)	0.82(02)	0.011(052)	...	0.01509	-19.48(14)	-0.08(15)
2008bf	-8.5	A	15.779(022)	-0.066(031)	0.87(04)	-0.023(059)	Y	0.02403	-19.36(09)	0.08(13)
2008bq	0.3	N	16.661(006)	0.052(008)	0.92(01)	0.090(051)	...	0.03400	-19.18(06)	-0.10(07)
2008fp	-3.7	A	13.829(020)	0.491(028)	0.84(05)	0.538(057)	...	0.00566
2008gl	-1.5	N	16.845(022)	0.050(031)	1.29(04)	0.043(059)	...	0.03402	-18.90(07)	-0.09(12)
2008gp	-6.0	...	16.455(031)	0.033(043)	0.97(11)	0.065(066)	...	0.03341	-19.28(08)	-0.19(16)
2008hj	-6.6	N	16.844(027)	0.005(038)	1.04(05)	0.028(063)	...	0.03789	-19.14(07)	-0.03(13)
2008hv	-6.6	A	14.799(006)	0.067(009)	1.25(01)	0.065(051)	Y	0.01255	-18.99(16)	-0.19(16)
2009D	-3.9	N?	15.789(016)	0.018(023)	0.84(03)	0.065(055)	Y	0.02501	-19.31(09)	-0.08(11)
2009F	-5.4	A	16.929(025)	0.635(036)	1.97(04)	...	Y	0.01296	-16.75(17)	-0.04(20)
2009I	-5.1	F	18.247(081)	0.702(115)	1.14(16)	0.713(125)	...	0.02617	-16.92(12)	0.22(36)
2009Y	-5.5	N?	14.042(032)	0.114(045)	0.88(06)	0.156(067)	...	0.00935	-19.09(22)	-0.16(26)
2009aa	-7.8	F?	16.355(023)	0.030(033)	1.12(04)	0.044(060)	Y	0.02731	-19.06(08)	-0.07(12)
2009ab	-10.2	A	14.652(046)	0.065(065)	1.21(09)	0.068(082)	...	0.01117	-18.65(21)	0.19(28)
2009ad	-8.3	...	16.074(096)	-0.006(136)	0.88(17)	0.036(145)	...	0.02840	-19.33(12)	-0.07(41)
2009ag	-3.5	F?	14.589(041)	0.241(058)	0.97(08)	0.273(077)	...	0.00864
2009cz	-4.1	N	15.786(053)	0.073(075)	1.05(10)	0.095(090)	...	0.02114	-19.06(11)	-0.13(25)
2009dc	-7.7	SC	15.141(066)	0.145(093)	0.59(11)	0.222(106)	...	0.02139	-19.68(12)	-0.61(29)

Notes. Columns: (1) SN name; (2) epoch of the first spectroscopic observation relative to B -band maximum light; (3) C II detection type (see Section 2.1): absorption (A); flat emission (F); no detection (N); (4) MW-extinction-corrected, K -corrected, apparent B -band peak magnitude (uncertainties in thousandth of mag); (5) observed pseudo-color at maximum light, corrected for MW reddening (uncertainties in thousandth of mag); (6) observed decline rate, $\Delta m_{15}(B)$ (uncertainties in hundredth of mag); (7) host galaxy color excess (uncertainties in thousandth of mag); (8) SNe with “Y” belong to the low-reddening sample; (9) heliocentric redshift from the NASA/IPAC Extragalactic Database (NED); (10) B -band absolute peak magnitude (uncertainties in hundredth of mag); (11) B -band Hubble residual (see Section 4; uncertainties in hundredth of mag).

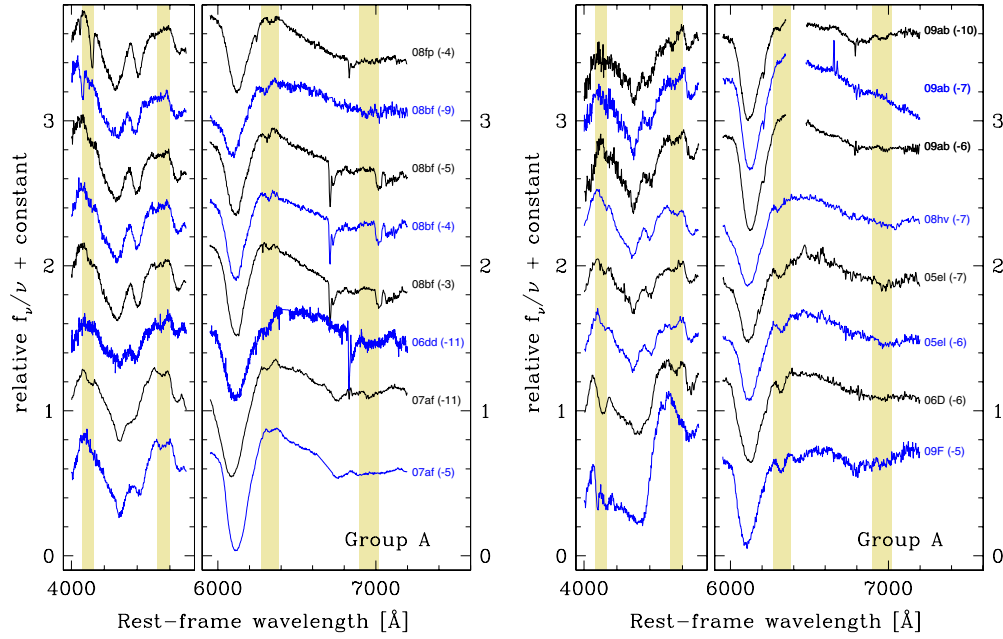


Figure 1. Spectra of all the SNe Ia classified in group A (with C II $\lambda 6580$ absorption) at the wavelength regions of the C II lines. The shaded bands mark the position of four C II lines blueshifted between 9000 and 14,000 km s⁻¹. For clarity, the spectra are plotted as f_ν/ν . Labels indicate the names of SNs and their age in days relative to B -band maximum light. The SNe are sorted from top to bottom in increasing order of $\Delta m_{15}(B)$. The gaps in the spectra of SN 2009ab (right panel) are due to a separation between two detectors.

(A color version of this figure is available in the online journal.)

Table 2
List of Pre-maximum Spectra

UT Date	MJD	Phase	Wavelength Range (\AA)	Resolution (\AA)	C II Class	pW(6300) (\AA)	References
(1)	(2)	(3)	(4)	(5)	(6)	(7)	(8)
SN 2004dt							
2004 Aug 12	53230.22	-8.7	4320-10315	...	N	<1.11	2
2004 Aug 12	53230.67	-8.2	3140-8589	...	N	<0.75	2
2004 Aug 13	53231.23	-7.7	3946-9702	...	N	<1.02	2
2004 Aug 13	53231.63	-7.3	3170-10250	...	N	<0.66	2
2004 Aug 15	53233.64	-5.3	3142-10400	...	N	<0.33	2
2004 Aug 15	53233.69	-5.3	3617-8879	...	N	<0.39	2
2004 Aug 16	53233.71	-5.2	3087-10211	...	N	<0.24	2
2004 Aug 16	53234.57	-4.4	3236-10678	...	N	<0.45	2
2004 Aug 18	53235.69	-3.3	3334-8878	...	N	...	2
2004 Aug 18	53236.54	-2.5	3217-10144	...	N	...	2
2004 Aug 19	53237.18	-1.8	3317-8894	...	N	...	2
2004 Aug 20	53238.22	-0.8	3318-8822	...	N	...	2
2004 Aug 21	53239.23	0.2	3337-8822	...	N	...	2

Notes. Columns: (1) UT date of the observation; (2) Julian date of the observation (JD - 2400000); (3) phase in days since B -band maximum light; (4) wavelength range covered; (5) spectral resolution in \AA as estimated from the FWHM of arc-lamp lines; (6) type of 6300 \AA feature (see Section 2.1); (7) pseudo-equivalent width of absorption at ≈ 6300 (3σ upper limits denoted with “<” sign); (8) references: (1) G. Folatelli et al. (2011, in preparation); (2) Altavilla et al. 2007; (3) Pastorello et al. 2007; (4) Taubenberger et al. 2008; (5) Yamanaka et al. 2009b; (6) Stritzinger et al. 2010; (7) this paper.

† Spectrum corrected to match photometry (see G. Folatelli et al. 2011, in preparation).

(This table is available in its entirety in a machine-readable form in the online journal. A portion is shown here for guidance regarding its form and content.)

observations, with small deviations which are not relevant to our analysis of carbon features. The ions producing the main spectral features are labeled (see Table 3). In some cases, “detached” components of Ca II and Fe II have been included to reproduce HV absorption features (Mazzali et al. 2005).

In the case of SN 2005el (see Figure 4), C II can be invoked to reproduce two absorptions observed at about 6300 and 7000 \AA .

The most evident of the two is C II $\lambda 6580$ which appears sharper in the data than in the calculations. The assumed distribution of C II is slightly “detached” by 500 km s⁻¹ above the photosphere in order to reproduce the location of the lines. The synthetic spectrum without C II (dotted line) fails to reproduce those two features. The identification of two absorptions provides extra support to the detection of carbon (see Section 2.4 for

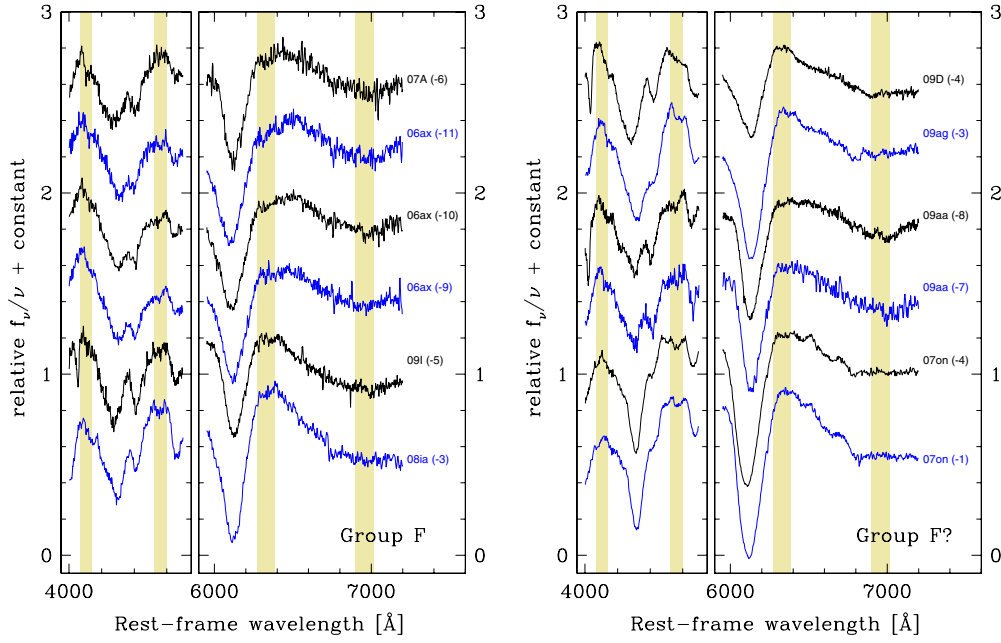


Figure 2. Left: spectra of all SNe Ia classified in group F (with flat Si II emission) at the wavelength regions of the C II lines. The shaded bands mark the position of four C II lines blueshifted between 9000 and 14,000 km s⁻¹. For clarity, the spectra are plotted as f_ν/ν . Labels indicate the names of the SNe and their age in days relative to B -band maximum light. The SNe are sorted from top to bottom in increasing order of $\Delta m_{15}(B)$. Right: the same for SNe Ia with F? classification.

(A color version of this figure is available in the online journal.)

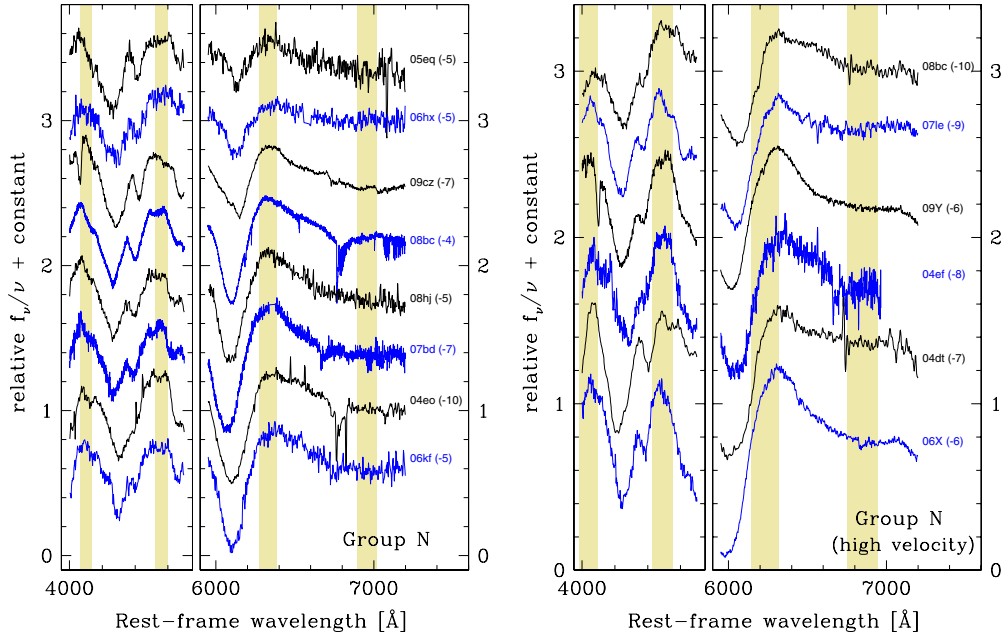


Figure 3. Left: spectra of all SNe Ia classified in group N (without signs of C II $\lambda 6580$) at the wavelength regions of the C II lines. The shaded bands mark the position of four C II lines blueshifted between 9000 and 14,000 km s⁻¹. For clarity, the spectra are plotted as f_ν/ν . Labels indicate the names of the SNe and their age in days relative to B -band maximum light. The SNe are sorted in increasing order of $\Delta m_{15}(B)$. Right: the same for SNe Ia with N classification and Si II expansion velocity greater than 13,500 km s⁻¹. In this case, the shaded bands mark the position of C II lines blueshifted between 12,000 and 20,000 km s⁻¹. The spectra are sorted from top to bottom in increasing order of Si II expansion velocity.

(A color version of this figure is available in the online journal.)

a comparison with other possible identifications). In the blue, only C II $\lambda 4745$ produces a detectable absorption in the synthetic spectrum. This line roughly matches an observed absorption, although the identification is not clear due to the presence of Si II and Fe III lines. Moreover, the synthetic spectrum in that region is dominated by an emission, which makes the identification even more doubtful. As will be shown below in the case of SN

2006ax, this emission could tentatively be suppressed by C III. No evident signature of C II $\lambda 4267$ is seen in either the observed or synthetic spectra at the expected position.

We refer the reader to a similar analysis done by Thomas et al. (2007) on SN 2006D which is also in group A according to our classification. The authors discuss whether non-LTE effects may modify the relative strength of C II lines to reproduce a strong

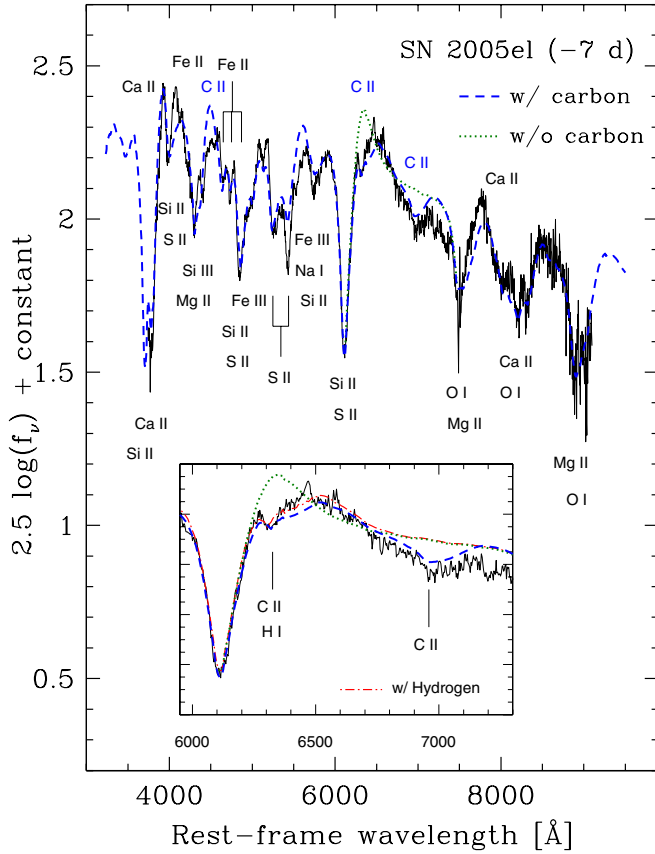


Figure 4. Spectrum of SN 2005el at -7 days (black solid line) which belongs to group A, and a matching SYNOW calculation (blue dashed line). The SYNOW synthetic spectrum without carbon is shown for comparison near the C II $\lambda 6580$ and $\lambda 7234$ lines (green dotted line). The labels indicate the main ions which contribute to the formation of the observed features. The most important contributors for each feature are labeled closest to the spectrum. Labels above the spectrum indicate that the ion was located “detached” from the photosphere. Inset: blow-up of the region around C II $\lambda 6580$ and $\lambda 7234$. The SYNOW spectrum containing H I instead of C II is also shown (red dotted line). The expected locations of C II and H α lines are indicated. While H I can reproduce the absorption at ≈ 6300 Å, C II produces a more solid identification by reproducing both absorptions at ≈ 6300 and ≈ 7000 Å.

(A color version of this figure is available in the online journal.)

and sharp absorption at about 4100 Å which is not identifiable with any other species.

The case of SN 2009F (see Figure 5) is similar to that of SN 2005el. As a consequence of SN 2009F being of the “Cool” type, the main differences in the synthetic calculations are a lower blackbody temperature, and larger O I and Ti II optical depths. Additionally, no ion—including C II—is detached from the photosphere. Again the synthetic spectrum with C II provides a better match to the observations than the one without carbon, in particular by reproducing observed absorptions near 6300 and 7000 Å, although the apparent width of the C II $\lambda 6580$ line is too wide in the calculations. The identification of C II lines in the blue part of the spectrum is even more difficult than in the case of SN 2005el due to the presence of strong Ti II lines.

Figure 6 shows the case of an F spectrum of SN 2006ax obtained 10 days prior to maximum light. In this case, even if the absorption feature is not evident, a comparison between the synthetic spectra with and without carbon clearly shows that the presence of C II is a plausible explanation for the flat emission component of the Si II $\lambda 6355$ line. A weak absorption near 7000 Å can be associated with C II $\lambda 7234$, as in the cases of SNe 2005el and 2009F. We thus assume a common origin for

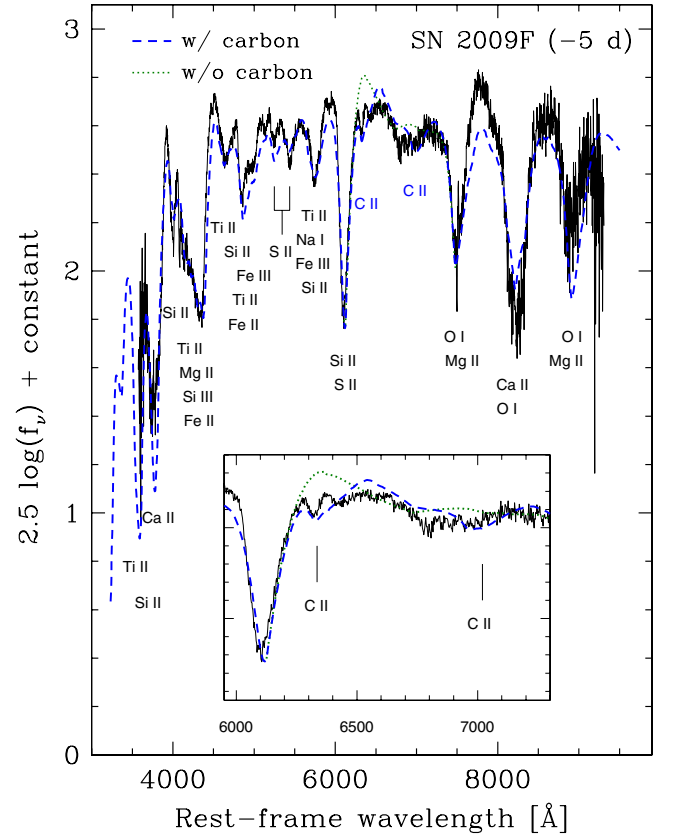


Figure 5. Spectrum of the “Cool” SN 2009F at -5 days (black solid line) which belongs to group A, and a matching SYNOW calculation (blue dashed line). The SYNOW synthetic spectrum without carbon is shown for comparison near the C II $\lambda 6580$ and $\lambda 7234$ lines (green dotted line). See Figure 4 for a description of the labels. Inset: blow-up of the region around C II $\lambda 6580$ and $\lambda 7234$. The expected locations of C II lines are indicated.

(A color version of this figure is available in the online journal.)

Table 3
Summary of SYNOW Parameters

Parameter	SN 2004eo	SN 2005el	SN 2006ax	SN 2009F
Age (days)	-6	-7	-10	-5
C II class	N	A	F	A
v_{ph} (km s $^{-1}$)	11,500	12,300	12,500	12,000
T_{BB} (K)	12,500	11,500	12,500	8,500
τ (C II)	0.04	0.1
τ (C II HV)	...	0.05
v_{min} (C II HV) (km s $^{-1}$)	...	12,800
τ (C III)	0.5	...
τ (O I)	0.7	0.5	0.1	1.5
τ (Na I)	0.2	0.1	0.1	0.5
τ (Mg II)	1.0	0.8	0.7	0.8
τ (Si II)	4.3	2.5	3.0	5.0
τ (Si III)	0.6	0.5	0.7	0.8
τ (S II)	1.5	1.0	0.8	0.5
τ (Ca II)	14.0	4.5	7.0	20.0
τ (Ca II HV)	2.0	1.0	2.5	...
v_{min} (Ca II HV) (km s $^{-1}$)	20,000	20,000	20,000	...
τ (Ti II)	0.3	1.0
τ (Fe II)	0.3	0.1	0.1	0.1
τ (Fe II HV)	0.4	0.2	0.3	...
v_{min} (Fe II HV) (km s $^{-1}$)	18,000	19,000	19,000	...
τ (Fe III)	1.0	0.5	0.6	0.5

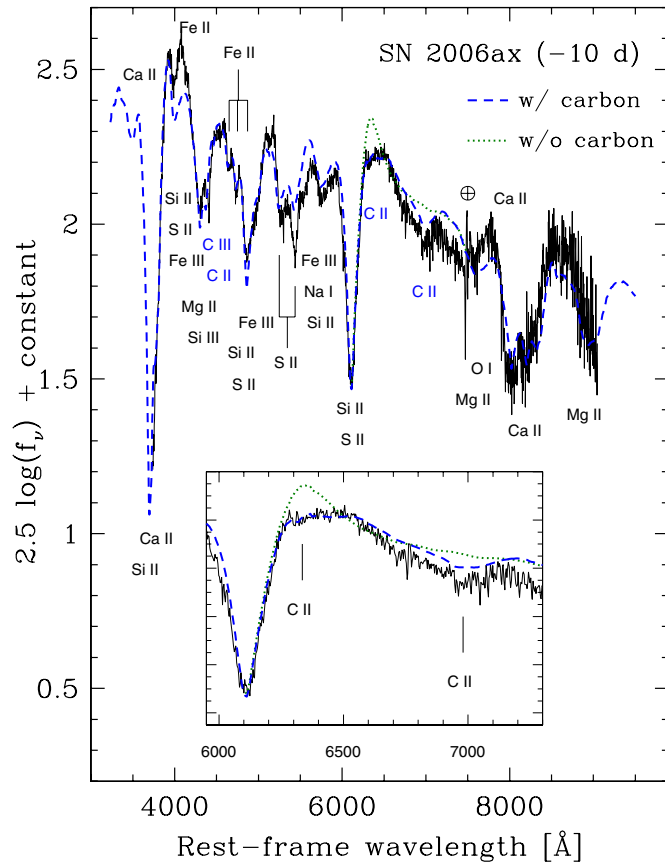


Figure 6. Spectrum of SN 2006ax at -10 days (black solid line) which is classified in group F, and a matching SYNOW calculation (blue dashed line). The SYNOW synthetic spectrum without carbon is shown for comparison near the C II $\lambda 6580$ and $\lambda 7234$ lines (green dotted line). See Figure 4 for a description of the labels. Inset: blow-up of the region around C II $\lambda 6580$ and $\lambda 7234$. The expected locations of C II lines are indicated.

(A color version of this figure is available in the online journal.)

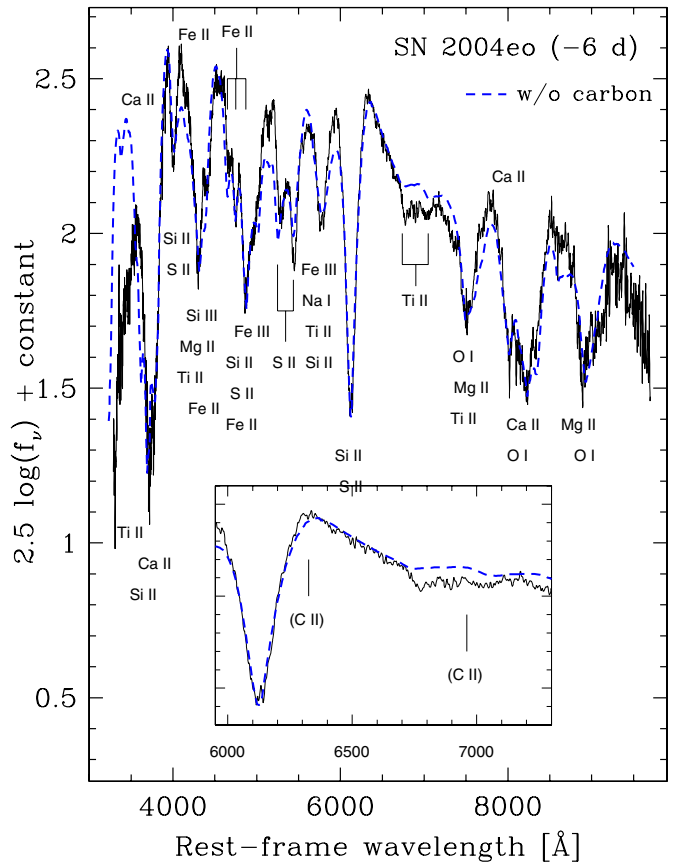


Figure 7. Spectrum of SN 2004eo at -6 days (black solid line) which belongs to the N class, and a matching SYNOW calculation without carbon (blue dashed line). See Figure 4 for a description of the labels. Inset: blow-up of the region around C II $\lambda 6580$ and $\lambda 7234$. The expected locations of C II lines at about 1000 km s^{-1} above the Si II velocity are indicated. The same as above for the spectrum of SN 2004eo at -6 days which belongs to the N class.

(A color version of this figure is available in the online journal.)

the spectral properties of A and F spectra in the range around 6300 \AA .

Note also in Figure 6 that we have tentatively included C III in the synthetic spectrum. This adds an absorption at about 4500 \AA due to C III $\lambda 4650$ which serves to suppress the emission components of Mg II and Si III lines to the blue. As mentioned above, C III can also be invoked to improve the fit in this wavelength region in the case of SN 2005el, as shown in Figure 4. Although the presence of C III $\lambda 4650$ has been considered previously in the literature (see Garavini et al. 2004; Branch et al. 2007; Parrent et al. 2011), its identification is only tentative because it would require a very high temperature to excite this transition (29.5 eV). It should be noted that more elaborate models, for example, those applied to the normal SN 2003du by Tanaka et al. (2011), do not involve the presence of C III lines even when some carbon is included in the ejecta.

For comparison, in Figure 7 we show the case of an N type spectrum. In this example, we show the spectrum of SN 2004eo obtained at -6 days along with a matching SYNOW spectrum. We see that, as opposed to the A and F cases, the match around 6300 \AA is good without the need to invoke C II. In a case like this we can confidently say that carbon is not detected. However, as shown in Section 2.2, in other cases classified as N or F?, carbon features may be hidden by noise or blending.

2.2. Detection Statistics

Assuming that the identification of the 6300 \AA feature in A and F SNe is C II, we see a remarkably large incidence of unburned material in the current sample. If we consider the objects with spectroscopy obtained before or at -4 days—the age of the oldest A spectrum—from a total of 32 normal SNe Ia we have nine objects in group A and three in group F. This means 38% of the SNe are in the A or F groups, and 28% in A. Apart from the recent work by Parrent et al. (2011) who find a similar detection fraction of 30%, previous claims for carbon in SNe Ia spectra have been sporadic (see Thomas et al. 2007; Branch et al. 2007). As shown below, we think this has to do with the relative scarcity of early-time spectra.

Moreover, we note that the fractions derived above are lower limits because we count as non-detections several cases where the data are not suitable to fully discard the presence of carbon. Below we present three different effects which can work against the detection of C II lines: noise, expansion velocity, and age.

2.2.1. Noise

Clearly, noise in the data can hide weak features such as the ones under study here. In order to quantify the detectability of the absorption at 6300 \AA , we have performed equivalent width measurements. Strictly speaking, since the location of the actual continuum is unknown, these are *pseudo-equivalent*

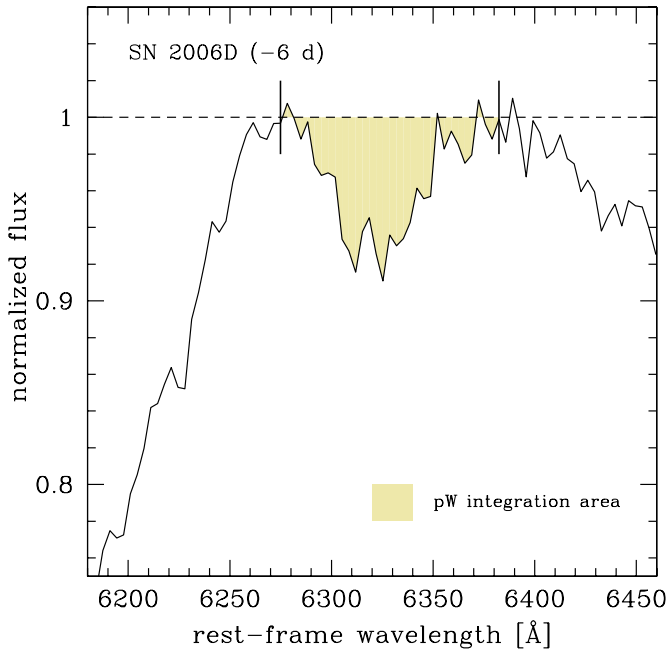


Figure 8. Example of a pseudo-equivalent width measurement (pW) for the C II $\lambda 6580$ line. A pseudo-continuum is defined as a straight line traced between the flux peaks on each side of the absorption feature (vertical lines). The spectrum is then normalized by this pseudo-continuum, and the pW is computed as the area of the normalized absorption (shaded region).

(A color version of this figure is available in the online journal.)

widths (pW). We simply trace a straight line along the absorption feature to mimic the continuum flux. An example of a pW measurement is shown in Figure 8. The pW is computed as the area of the absorption feature after normalizing the spectrum by a local pseudo-continuum. In cases when no absorption is seen, we derive an uncertainty in the pW value in the region around 6300 Å in order to set a 3σ upper limit. The measured values and upper limits are listed in Table 2, and shown in Figure 9.

We can see that, in general, $pW \gtrsim 1$ Å for objects in the A and F groups, and that most of the 3σ upper limits of SNe with no C II detections lie below that value. However, in several cases the upper limits are comparable to or even larger than the measured pW of objects in groups A and F. This implies that some of the SNe Ia with carbon may have gone undetected because of noise in the spectra.

2.2.2. Expansion Velocity

The higher the expansion velocity, the wider the spread of spectral features in wavelength space, and thus the larger the impact of line blending. In particular, the hypothetical 6300 Å absorption, which is much weaker than its neighboring Si II $\lambda 6355$ line, would become increasingly blended into the red absorption wing of the latter. This would make the detection of carbon problematic when expansion velocities are high.

To illustrate this problem, plotted in Figure 10 are synthetic spectra obtained with SYNOW using different photospheric velocities. For comparison, data of different SNe with approximately matching expansion velocities are shown along with the synthetic spectra. The top synthetic spectrum was tailored to match the observed one of SN 2006D at -6 days. We note that the C II $\lambda 6580$ absorption in the synthetic spectrum is wider than the observed one, but it reproduces well the observed intensity. This SYNOW spectrum is taken as the fiducial model to produce the rest of the synthetic spectra shown in the figure.

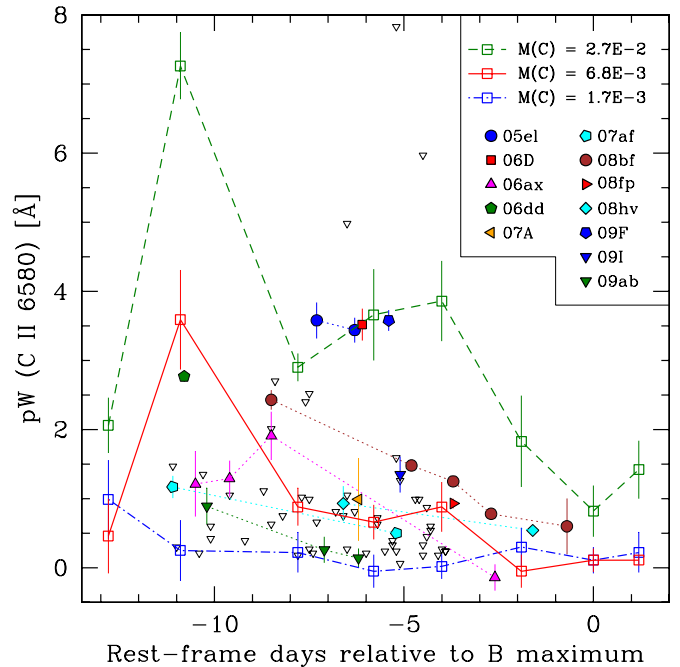


Figure 9. Pseudo-equivalent width of the absorption at ≈ 6300 Å which is attributed to C II $\lambda 6580$. Filled symbols are used for SNe Ia in A and F groups. Open triangles mark 3σ upper limits for the rest of the spectra in the current sample. Open squares linked with lines show the results for synthetic spectra computed for different masses of carbon in the velocity range $10,500 \text{ km s}^{-1} < v < 15,000 \text{ km s}^{-1}$ (see Section 2.3).

(A color version of this figure is available in the online journal.)

In each case we have only varied the photospheric velocity and optical depth of Si II in order to match the location and strength of the Si II $\lambda 6355$ absorption. Note that we have not attempted to produce an accurate match of each spectrum, but have only tried to illustrate the effect of Doppler blending.

It is clear from Figure 10 that, when the expansion velocity exceeds roughly $15,000 \text{ km s}^{-1}$, a C II absorption as strong as or weaker than the one of SN 2006D would be very difficult to detect. In the case of SN 2004ef at -6 days, the signal-to-noise ratio of the data makes the detection of the hypothesized C II line barely possible. For SN 2007le at -9 days, we can observe some “wiggles” on the Si II $\lambda 6355$ emission profile which may be compatible with a C II absorption. These weak features, along with the complex structure of the Si II absorption, disappear by the following observation of SN 2007le obtained at -4 days. This led to our classification of this object as “F?”

The right-hand panel of Figure 3 shows several cases of non-detections of C II for SNe Ia with Si II velocities above $13,500 \text{ km s}^{-1}$. In some of these cases, specifically for SNe 2004dt and 2006X, the expansion velocities are so large that they would hide the weak C II absorption observed in the case of A-type SNe Ia. We note that the nature of SN Ia explosions conspires with this effect against the detection of carbon. This is because expansion velocities are greatest at the earliest phases, which implies that the line blending effect is worst at times when the plausible C II absorption is expected to be strongest (see Section 2.2.3).

As shown in Section 3, none of the spectra classified as A or F show a Si II $\lambda 6355$ velocity greater than $\approx 12,500 \text{ km s}^{-1}$. According to the brief analysis based on Figure 10, the detection of the C II $\lambda 6580$ line could be possible for velocities above that value and up to $\approx 15,000 \text{ km s}^{-1}$. This may indicate that

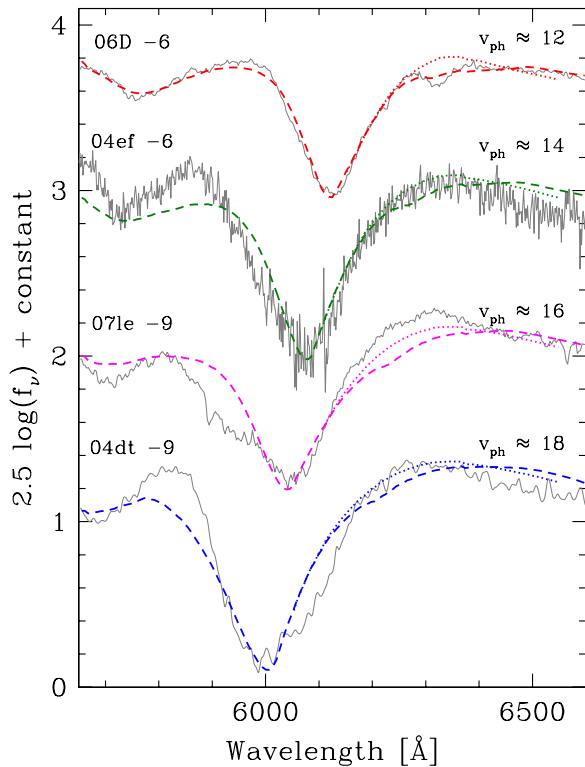


Figure 10. Effect of Doppler blending on the possible detection of C II $\lambda 6580$. Four observed spectra are plotted (gray continuous lines) with the labels on the left side indicating the SN name and epoch in days relative to B maximum. SYNOW calculations accompanying each spectrum show the cases with (dashed lines) and without (dotted lines) C II. The top synthetic spectrum was produced to fit the complete observed spectrum of SN 2006D at -6 days. This fiducial spectrum was used to produce the other synthetic spectra with different photospheric velocities. The labels on the right indicate this velocity in units of 10^3 km s^{-1} .

(A color version of this figure is available in the online journal.)

the lack of carbon detections among spectra within this range of expansion velocities is not exclusively due to the effect of Doppler blending.

2.2.3. Age

All the claimed detections of C II in the spectra of normal SNe Ia, as the ones presented in this paper and in previous publications (Thomas et al. 2007; Branch et al. 2007; Parrent et al. 2011), correspond to early-time observations, most commonly between one and two weeks before maximum light. This is mainly because carbon is expected to be present in the outer region of the ejecta which are visible at early phases. This is consistent with the temporal decrease in the strength of the absorption at $\approx 6300 \text{ \AA}$, as can be seen in Figure 9. The case of SN 2008bf, shown in the left panel of Figure 1, is a clear example of this evolution between -9 and -3 days. An additional spectrum of this SN, obtained at -1 day, is classified as N (see Table 2).

Sample statistics further support this picture. Figure 11 shows the fraction of carbon detections as a function of age for the current sample. The fractions are simply the ratio of the number of SNe in group A (or A and F) to the total amount of objects whose spectra cover the region around 6300 \AA . As we go from -11 to -1 day, the fraction decreases monotonically from about 30% (40% for A+F) to zero detections.

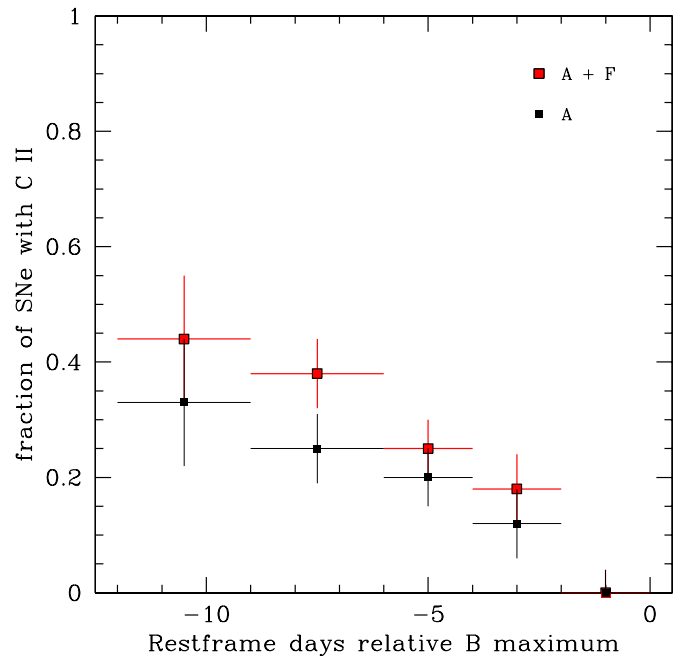


Figure 11. Fraction of SNe with C II as a function of age. Values show the ratio of SNe with spectra in the A (solid black) or A+F (shaded red) groups to the total number of SNe with spectra covering the region around 6300 \AA . Horizontal error bars show the size of the epoch boxes used for computing statistics. Vertical error bars indicate the expected variation of the fraction for an assumed error of ± 1 SN with carbon.

(A color version of this figure is available in the online journal.)

In the next section we show that some models predict a weaker absorption at $\approx 6300 \text{ \AA}$ before -11 days, which may lead to a lower detection fraction prior to that epoch. This highlights the importance of early observations in determining the incidence of unburned material in the ejecta of SNe Ia.

2.3. The Mass of Carbon

In an attempt to put constraints on the amount of unburned material which is necessary to explain the observed spectral features, we have computed synthetic spectra using the Monte Carlo code developed by Mazzali & Lucy (1993) and updated by Lucy (1999) and Mazzali (2000). A recent description of the code and its approximations was given in an analysis of SN 2003du by Tanaka et al. (2011). For that standard SN (Stanishev et al. 2007) the authors find that a mass of carbon of $M(C) = 6.8 \times 10^{-3} M_{\odot}$ (mass fraction $X(C) = 0.002$) in the velocity range $10,500 \text{ km s}^{-1} < v < 15,000 \text{ km s}^{-1}$ is suitable to explain the suppressed emission peak of the Si II $\lambda 6355$ line observed at -11 days. More carbon is expected to be present in outer layers, but it would not produce any noticeable effect in the spectrum (see Figure C1 of Tanaka et al. 2011). The authors set an upper limit of $0.016 M_{\odot}$ for the total mass of carbon in the ejecta of SN 2003du. Based on this configuration we produce two additional models by only changing the mass of carbon in the velocity range given above to four times below and above the fiducial value of $M(C) = 6.8 \times 10^{-3} M_{\odot}$. The three models are employed to compute synthetic spectra at several phases between -13 and $+1$ days from maximum light and thus evaluate the effect on the C II $\lambda 6580$ line.

Figure 9 shows the pW of C II $\lambda 6580$ as a function of SN phase for the synthetic spectra of different carbon mass. As expected, the pW generally grows with mass. The range of observed pW is well represented by the assumed range of $M(C)$. The lowest

adopted mass ($1.7 \times 10^{-3} M_{\odot}$) would correspond to SNe with no carbon detection, while the largest mass ($2.7 \times 10^{-2} M_{\odot}$) roughly matches the strongest observed C II 6580 lines for SNe in group A at about one week before maximum light.

In general, the models confirm the observed fact that the pW of carbon tends to decrease with phase. The exception to this is the increase in pW between the modeled spectra at -13 and -11 days. Close inspection of the synthetic spectra at -13 days shows a strong emission component of the Si II line which washes away the weak absorption due to C II and produces a low pW as compared with that at -11 days. To a lower extent, the C II pW is additionally reduced by the fact that at -13 days part of the carbon lies below the photosphere. Furthermore, a relatively larger expansion velocity at day -13 enhances line blending, thus contributing to the decrease in the measured pW. If this effect were generally valid, one would expect that the fraction of SNe with carbon detection should *decrease* at phases earlier than roughly -12 days. It should be noted, however, that the adopted model produces a worse match to the observed spectrum of SN 2003du at -13 days than at later phases (see Figure 2 of Tanaka et al. 2011), especially in the wavelength region under scrutiny here. Unfortunately, our data do not cover such early phases and thus we cannot corroborate the results of the model. More early-time spectroscopy of SNe Ia is needed to settle this question.

2.4. Hydrogen?

With the aid of SYNOW we have studied alternative identifications for the absorption around 6300 \AA in A-type SNe Ia. Other ions which may produce such absorption at expansion velocities near the photospheric value are Ne I and H I. The strongest Ne I lines (at 6402 and 6506 \AA) would only reproduce the absorption at $\approx 6300 \text{ \AA}$ if the expansion velocity were between 4000 and 9000 km s^{-1} . Such velocities are lower than those observed for SNe Ia before maximum light.

On the other hand, H I is a plausible alternative (Lentz et al. 2002). H-rich material may be present by mass transfer from a companion star in a single-degenerate progenitor system. If the observed absorption were due to H I this would rule out the double-degenerate scenario for a fraction of SNe Ia.

As can be seen in the inset plot of Figure 4 (dotted lines), $H\alpha$ at photospheric velocity is able to reproduce the 6300 \AA absorption as well as C II does. The weaker absorption at about 7000 \AA is, however, not reproduced. This makes the identification of H I less plausible than that of C II. With the given optical depth for $H\alpha$, the expected strength of $H\beta$ is barely detectable, and it is not observed in the data.

We have computed Monte Carlo synthetic spectra including H in order to model the observations. For this purpose we utilized the abundance distribution derived for SN 2003du at -11 days as given by Tanaka et al. (2011). We added H with mass fraction up to 0.1 in the range of $10,500 \text{ km s}^{-1} < v < 15,000 \text{ km s}^{-1}$ —i.e., right above the photosphere. We found that the absorption at 6300 \AA for SNe in the A group can be reproduced with mass fractions $X(\text{H}) \sim 0.05$ which in this case translates into a total hydrogen mass of $M(\text{H}) \sim 10^{-2} M_{\odot}$. This is a very large amount of hydrogen which is incompatible with the theoretical picture of SNe Ia. In the single-degenerate scenario, models of progenitors with mass transfer predict an upper limit of $\sim 10^{-7} M_{\odot}$, which is set by the ignition mass of H (Nomoto et al. 2007). In the double-degenerate scenario, an even smaller amount of hydrogen is expected.

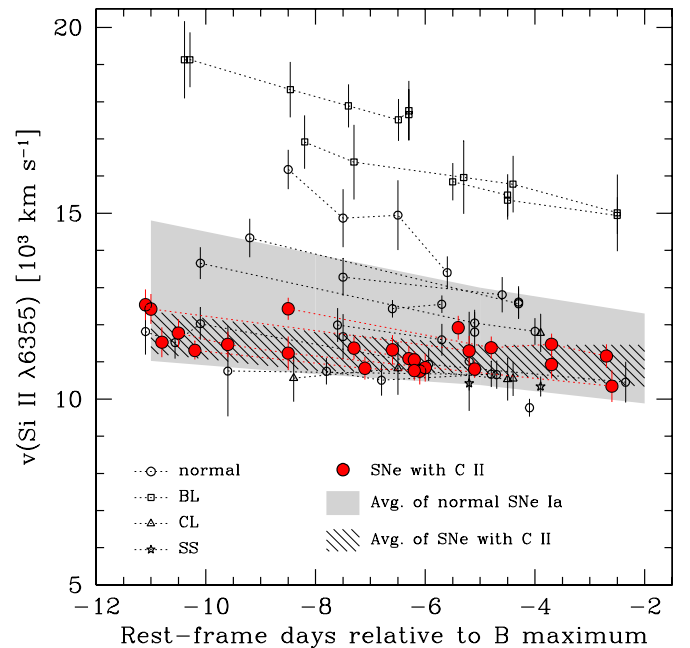


Figure 12. Expansion velocities of Si II $\lambda 6355$ as a function of epoch relative to B maximum. Open black symbols mark SNe without carbon, with different shapes for different spectral subtypes as given by G. Folatelli et al. (2011, in preparation). Filled symbols are used for SNe in the A and F groups. These symbols are the same as in Figure 9. Data points for the same SN are linked with dotted lines. The shaded gray region marks the region within 1σ about the average velocity evolution of normal SNe Ia as given by G. Folatelli et al. (2011, in preparation). The yellow hashed region indicates the average and 1σ region for SNe with carbon.

(A color version of this figure is available in the online journal.)

Alternatively, a mass of the order of $0.01 M_{\odot}$ of hydrogen could be stripped from the companion star in the single-degenerate scenario (Marietta et al. 2000; Pakmor et al. 2008). However, according to these simulations, the stripped hydrogen is distributed in the inner layers ($v < 4000 \text{ km s}^{-1}$; Pakmor et al. 2008), which are not visible in early-time spectra.

Based on these observational facts and theoretical predictions, even if the 6300 \AA absorption can be reproduced by hydrogen, we consider this possibility to be unlikely in favor of the C II identification.

3. SPECTROSCOPIC PROPERTIES

We now compare the spectral properties of the samples of SNe with and without evidence of carbon. We first examine the expansion velocities. Figure 12 shows Si II $\lambda 6355$ expansion velocities as derived from the blueshift of the absorption minimum. We see that the sample of normal SNe Ia with carbon appear to lie preferentially near the lower edge of the velocity distribution of the complete sample. Si II velocities are below $\approx 12,500 \text{ km s}^{-1}$ in all of these cases. In terms of the classification by Benetti et al. (2005), none of the SNe with carbon are of high-velocity-gradient (HVG) type. Accordingly, none of the SNe with carbon belong to the “Broad-line” (BL) type as defined by Branch et al. (2006; see also G. Folatelli et al. 2011, in preparation). As explained in Section 2.2.2, the lack of carbon detection when velocities are high may be caused by an observational bias as a consequence of Doppler blending. However, the fact that in our simulations C II lines are expected to be noticeable up to velocities of $\approx 15,000 \text{ km s}^{-1}$ suggests that the preference for low velocities is real and not completely

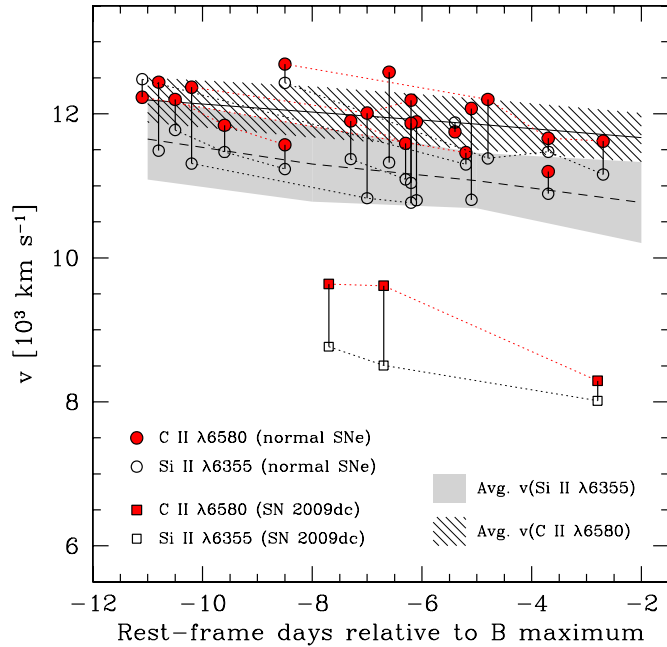


Figure 13. Expansion velocities of C II $\lambda 6580$ (filled symbols) and Si II $\lambda 6355$ (open symbols) as a function of epoch relative to B maximum. The dashed line marks the average Si II $\lambda 6355$ velocity and the gray shaded area indicates the 1σ dispersion. The solid line and hashed region mark the average and 1σ dispersion of C II $\lambda 6580$ velocities, respectively. SN 2009dc is excluded from both averages.

(A color version of this figure is available in the online journal.)

due to the observational bias. The possible implications of the velocity of carbon on SNe Ia models are briefly discussed in Section 5.

Signatures of carbon are not exclusively found in normal SNe Ia. In our sample, one fast-declining object, SN 2009F, belongs to group A (see Figure 5). In the classification scheme of Branch et al. (2006), this SN is of the “Cool” type. Three other CL SNe were observed at the range of epochs considered here, with no evidence of C II lines. The two SNe of the “shallow silicon” type with early-time spectroscopy do not show evidence of carbon.

In Figure 13 we present the expansion velocities of the bulk of carbon, measured from the absorption minimum located at $\approx 6300 \text{ \AA}$, under the assumption that it is due to C II $\lambda 6580$. On average, the evolution of C II $\lambda 6580$ velocities is parallel to that of Si II $\lambda 6355$ velocities, and lying at $\approx 1000 \text{ km s}^{-1}$ above. These velocities indicate that carbon appears slightly detached above the photosphere (see Section 2.1). If carbon were left unburned by a spherically symmetric explosion, then it would be expected to only be present in the outermost regions of the ejecta (e.g., Nomoto et al. 1984 and Iwamoto et al. 1999 predict a minimum velocity of $15,000 \text{ km s}^{-1}$). For current one-dimensional deflagration and delayed-detonation models, no carbon should be left at such low velocities. As discussed in Section 5, multi-dimensional effects may account for the presence of carbon deep in the ejecta.

If the detection of carbon is related to prevalent asymmetries in the ejecta, we would expect to find evidence of other effects of asphericities. In addition to the distinction between LVG and HVG SNe which was suggested as evidence of asymmetries (Maeda et al. 2010a), another possible effect would be the presence of HV components in the spectra (Tanaka et al. 2006). As was shown in Section 2.1, at the SN phases studied here,

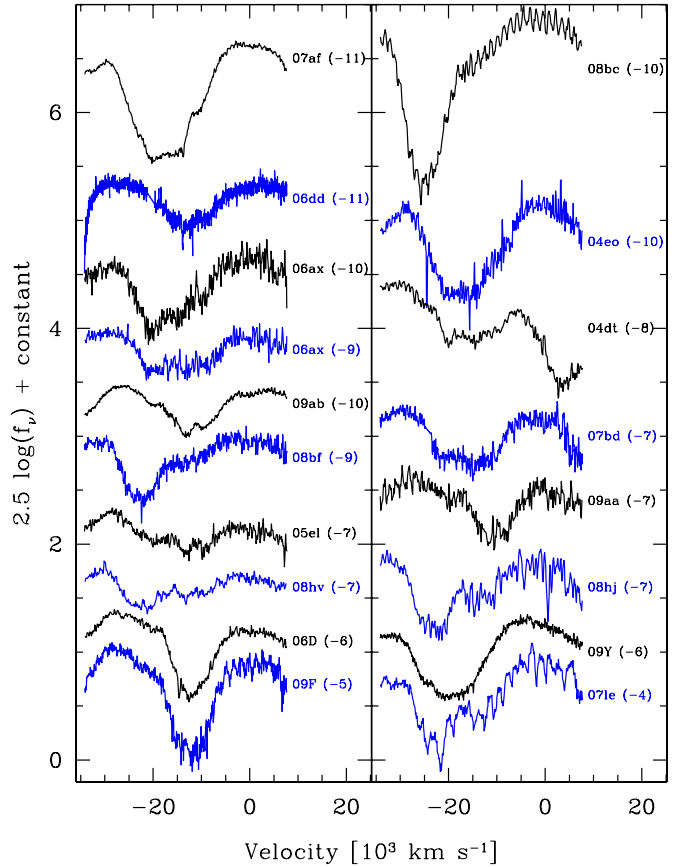


Figure 14. Spectra in the region of the Ca II IR triplet as a function of Doppler velocity assuming 8579 \AA as the effective rest wavelength. Left panel: spectra classified in A and F groups. Right panel: spectra of type N. The spectra are sorted according to their age (which is given in parentheses). We see that cases with and without strong high-velocity components—near $20,000 \text{ km s}^{-1}$ —are present in both groups of SNe Ia.

(A color version of this figure is available in the online journal.)

HV components of Ca II and Fe II are commonly seen (see also Mazzali et al. 2005). Figure 14 shows, however, that the presence or absence of HV Ca II infrared (IR) triplet absorption is not obviously related to the presence of carbon.

3.1. Super-Chandrasekhar SNe

As a comparison we examine the CSP spectra of the peculiar SN 2009dc. This SN exhibits strong carbon features in its pre-maximum spectra, which are also present until approximately a week after maximum. From its spectral properties, slow light curves, and exceedingly high luminosity, it has been suggested that SN 2009dc resulted from a super-Chandrasekhar mass progenitor (Yamanaka et al. 2009a; Tanaka et al. 2010; Silverman et al. 2011; Taubenberger et al. 2011).

In Figure 12, we compare the expansion velocities of Si II $\lambda 6355$ and C II $\lambda 6580$ derived from the spectra of SN 2009dc to our sample of normal SNe Ia. This figure illustrates that SN 2009dc has lower Si II velocities than the normal objects by $\approx 2000 \text{ km s}^{-1}$. Interestingly, the relation between C II and Si II velocities that was observed for normal SNe Ia also holds for SN 2009dc. In this case, the bulk of carbon also appears to be located above the silicon layer by $\approx 1000\text{--}2000 \text{ km s}^{-1}$. From a study of a different sample of SNe Ia, including a few super-Chandrasekhar candidates, Parrent et al. (2011, see their Figure 8) found a similar agreement of the relative location of

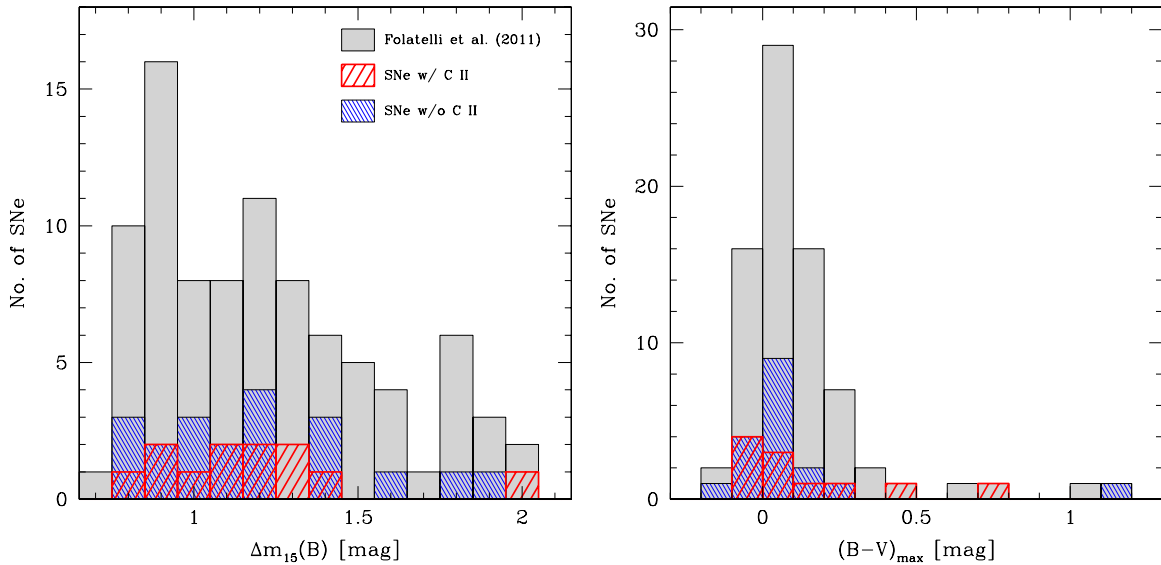


Figure 15. Left: distribution of light-curve decline rates, $\Delta m_{15}(B)$, for SNe Ia with carbon (black hashed), without carbon (light gray hashed), and the complete sample of G. Folatelli et al. (2011, in preparation) (solid gray). Right: distribution of observed $(B - V)$ pseudo-colors at maximum light for SNe Ia with $\Delta m_{15}(B) \leq 1.6$ mag. The shading code is the same as in the left panel.

(A color version of this figure is available in the online journal.)

carbon and silicon layers. This is an interesting finding because it may indicate that, even if the progenitors may be very different, the explosion produces similar relative distribution for the bulk of these elements.

4. PHOTOMETRIC PROPERTIES

This section presents a comparative analysis of the photometric properties of SNe Ia with and without signatures of carbon in the early-time spectra. For this purpose, a sample of 32 normal SNe Ia was selected with spectra obtained earlier than four days before maximum light. Twelve of these objects belong to groups A and F, which are the ones considered to show carbon in their ejecta. We base this study on the photometric data published by Contreras et al. (2010) and Stritzinger et al. (2011). The data were analyzed with the SNooPy package (Burns et al. 2011) in order to derive light-curve parameters such as times and magnitudes at maximum light, and B -band decline rates ($\Delta m_{15}(B)$; Phillips 1993).

4.1. Decline Rate and Color

Figure 15 (left panel) shows the distribution of light-curve decline rates, $\Delta m_{15}(B)$, for both groups. As a reference, we also show the distribution of the complete sample of G. Folatelli et al. (2011, in preparation). The group of SNe Ia with carbon covers a wide range of decline rates, including a fast-declining (1991bg-like) event. The average decline rate of all three samples (i.e., the complete sample, and those with and without carbon) is 1.2 ± 0.3 mag. Unfortunately, the sample sizes are too small to pursue a robust statistical test of the similarity among the distributions.

Shown in the right-hand panel of Figure 15 is the distribution of observed $(B - V)$ pseudo-colors at maximum light for SNe Ia with and without carbon, and for the reference sample. To avoid confusion with the intrinsically red CL subclass of SNe Ia, we have excluded all SNe with $\Delta m_{15}(B) > 1.65$ mag. We can see a tendency in the distribution of SNe with carbon to peak at a bluer color, although the statistics may be affected by the small number of cases. As pointed out recently (Pignata et al.

Table 4
Fits of Intrinsic $(B - V)$ Pseudo-color versus Decline Rate

Sample (1)	a (2)	b (3)	σ_f (4)	N_{SNe} (5)
With carbon	-0.023 ± 0.028	0.31 ± 0.15	0.06 ± 0.05	6
Without carbon	0.020 ± 0.018	-0.01 ± 0.07	0.03 ± 0.04	6
All	-0.002 ± 0.018	0.09 ± 0.08	0.05 ± 0.02	12
Folatelli et al. (2010)	-0.02 ± 0.01	0.12 ± 0.05	...	14

Notes. Fits of the type: $(B - V)_0 = a + b[\Delta m_{15}(B) - 1.1]$ for $\Delta m_{15}(B) \leq 1.6$ mag. Columns: (1) sample of SNe; (2) fit intercept; (3) fit slope; (4) intrinsic dispersion of fit (in magnitudes; see Section 4); (5) number of SNe used in fit.

2008; Wang et al. 2009; Foley & Kasen 2011; Maeda et al. 2011), SNe Ia with high expansion velocities tend to show redder colors at maximum light. Tanaka et al. (2008) suggested that the underlying cause of the difference in colors between HVG and LVG SNe is a variation in effective temperature which arises from a difference in photospheric velocity. The fact that SNe with carbon are all low-velocity objects may cause the observed difference in the color distributions.

In order to further study possible differences in the intrinsic colors of SNe Ia with and without carbon, we have selected those objects in each group which can be considered to have suffered little reddening. Following the criteria of Folatelli et al. (2010), we picked SNe that (1) occurred in E/S0 galaxies or that appeared outside the nuclei and arms of spiral galaxies and (2) which did not show any sign of interstellar Na I D absorption in their early-time spectra. To these we added a few objects whose observed $(B - V)$ colors one month past maximum light were compatible with the intrinsic-color law given in Equation (2) of Folatelli et al. (2010). The SNe in this low-reddening sample are indicated with a “Y” in column 8 of Table 1.

Figure 16 shows the relation between color and decline rate for this sample of low-reddening SNe, with and without carbon absorption. Table 4 lists the resulting parameters of the straight-line fits performed on different subsamples. We have adopted a Markov Chain Monte Carlo (MCMC) approach to

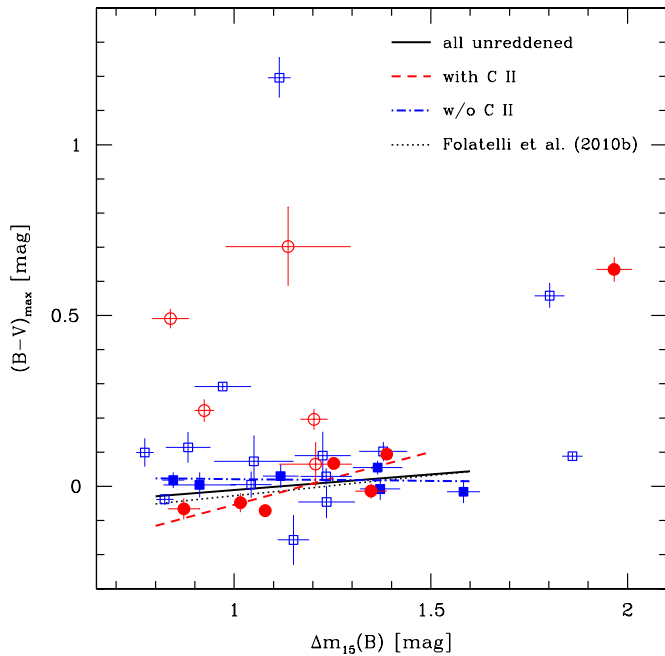


Figure 16. $(B - V)$ pseudo-colors at maximum light vs. $\Delta m_{15}(B)$. Solid symbols indicate SNe Ia with low reddening (see the text). Circles mark SNe with carbon and squares mark SNe without carbon. Straight-line fits to low-reddening objects are shown with a dashed line for SNe with carbon, dot-dashed line for SNe without carbon, and solid line for both groups together. The dotted line is the fit given by Folatelli et al. (2010) using a different sample.

(A color version of this figure is available in the online journal.)

perform the fits, with a full covariance matrix representation of the uncertainties in $(B - V)$ and $\Delta m_{15}(B)$. We have also added an “intrinsic dispersion” term, σ_I , to the uncertainties which accounts for the extra dispersion in the data with respect to the straight-line fit. This term is left as a free parameter and its resulting values are given in Table 4. The “uncertainties” in σ_I provide an estimate of the precision to which the MCMC method can determine this intrinsic dispersion. Note that once again the CL SNe have been excluded by requiring $\Delta m_{15}(B) \leq 1.6$ mag.

As shown in Table 4 and Figure 16, the relation between color and decline rate for the combined sample of SNe with low-reddening is compatible with the fit given by Folatelli et al. (2010). On the other hand, if the sample is divided between those SNe with carbon and those without, a steeper relation is found for the former than for the latter SNe. Based on the posterior probability distributions resulting from the MCMC analysis, we find that the intercepts and slopes of both fits are different at the 80% and 90% confidence levels, respectively. We must note that all of the SNe used in the fits—those which are assumed to be unreddened—happen to belong to the low-velocity-gradient (LVG) class, so the difference cannot be explained by color variations between LVG and HVG SNe. Clearly, this difference must be confirmed using a larger SN sample.

4.2. Luminosity

Now we compare the luminosities of SNe Ia with and without carbon. For this purpose, we compute distance moduli based on the redshifts and assuming a standard $\Omega_M - \Omega_\Lambda$ model of the universe (see Equation (5) of Folatelli et al. 2010), which is accurate enough for the range of redshifts in the current sample. To avoid uncertainties larger than about 10% in the distances

due to peculiar motions of galaxies in the local universe, the sample is cut by imposing that $z > 0.01$.

Figure 17 shows the histograms of B -band absolute peak magnitudes corrected for Milky Way and host-galaxy extinction. In order to derive the latter correction, color excesses $E(B - V)$ were computed from the differences between observed $(B - V)$ pseudo-colors at maximum light and the law of intrinsic color versus $\Delta m_{15}(B)$ provided by Folatelli et al. (2010). Color excesses were converted into extinctions by multiplying by a total-to-selective absorption coefficient equivalent to the Galactic average of $R_V = 3.1$. To avoid large uncertainties in the extinction correction, on the left panel of Figure 17 we cut the sample by requiring that $(B - V)_{\max} < 0.2$ mag, after correcting for Milky Way extinction. We note an apparent difference in the extinction-corrected peak luminosities in the sense that SNe Ia with carbon are on average *fainter* than those without, and also than the reference sample. This difference is however statistically marginal. The values are $\langle M_B^0 \rangle = -19.25 \pm 0.33$ mag for 55 objects in the reference sample, and $\langle M_B^0 \rangle = -19.23 \pm 0.38$ mag for 15 SNe with no carbon detection. For the six SNe with carbon, this value is $\langle M_B^0 \rangle = -19.10 \pm 0.21$ mag, i.e., 0.13 mag fainter but well within the dispersion.

A similar effect is seen in the histograms of the right-hand panel of Figure 17, where extinction-corrected, absolute peak magnitudes are shown, this time including objects with $(B - V)_{\max} \geq 0.2$ mag, but adopting a low value of the total-to-selective absorption coefficient of $R_B = 2.74$, as derived from Hubble fits by Folatelli et al. (2010). The differences in luminosity may in part be due to inaccurate extinction corrections caused by a difference in intrinsic colors as that seen in Figure 16. If, as suggested by Figure 16, SNe with carbon show bluer intrinsic colors then the extinction corrections for this group would be underestimated. In fact, if we adopt a different extinction correction for each group of SNe based on the intrinsic-color laws given in Table 4, the differences in average extinction-corrected peak magnitudes nearly vanish. This may indicate that the differences between both groups are related to differences in intrinsic colors rather than intrinsic luminosities.

In Figure 18, we show the distributions of Hubble residuals in B band, ΔM_B . For this purpose, we adopted the parameters of Fit 2 in Table 8 of Folatelli et al. (2010) which correspond to a fit of distance moduli versus $\Delta m_{15}(B)$ and $(B - V)$ pseudo-colors. The discrepancy between SNe with and without carbon in this case is seen in the same direction as above, although reduced to 0.08 mag. The mean residuals and their standard deviations are $\langle \Delta M_B \rangle = 0.03 \pm 0.18$ mag and $\langle \Delta M_B \rangle = -0.05 \pm 0.21$ mag for SNe Ia with and without carbon, respectively.

Finally, we consider the effect of reddening on absolute peak magnitudes. For this purpose, we take the values of M_V at maximum light corrected for decline rate by adopting the slope of fit 7 in Table 9 of Folatelli et al. (2010). In Figure 19, we show these corrected peak magnitudes versus $E(B - V)$ color excesses derived as explained above. With the current sample, we find no evidence of different extinction properties between SNe Ia with and without carbon. The data favor a low value of $R_V \approx 2.1$ as has been found in previous studies of SNe Ia data.

5. DISCUSSION AND CONCLUSIONS

The most striking result of this paper is the large incidence of carbon lines in SNe Ia. In the CSP sample, we have

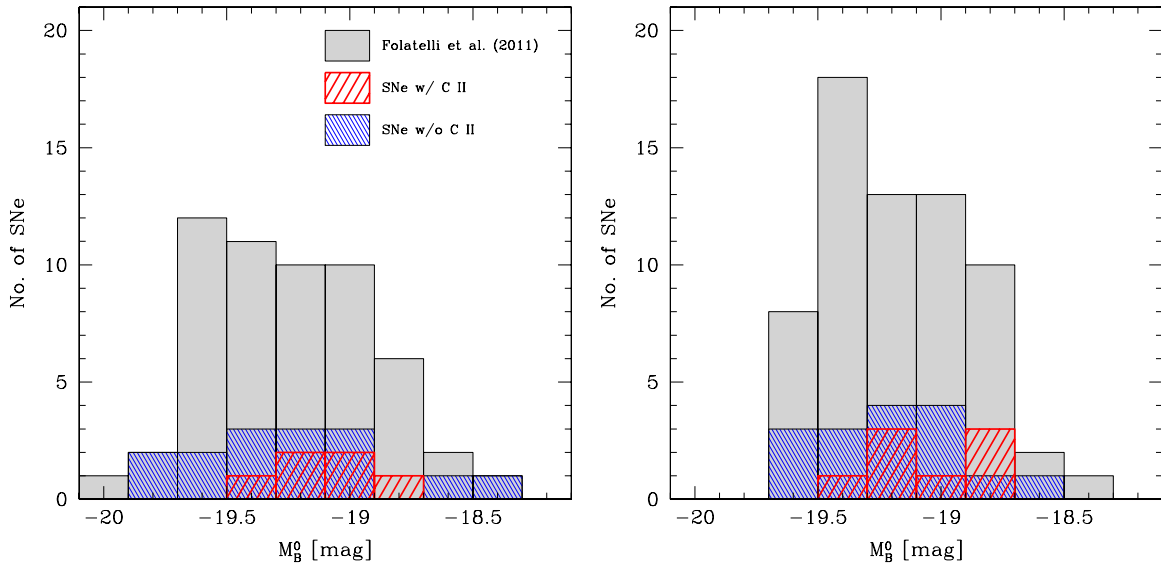


Figure 17. Distributions of extinction-corrected B -band absolute peak magnitudes. Left: extinction corrections derived using $R_V = 3.1$ and cutting the sample so that $(B - V) < 0.2$ mag. Right: including the complete range of $(B - V)$ colors, but adopting a low value of $R_B = 2.74$ (Folatelli et al. 2010). The shading code is the same as in Figure 15.

(A color version of this figure is available in the online journal.)

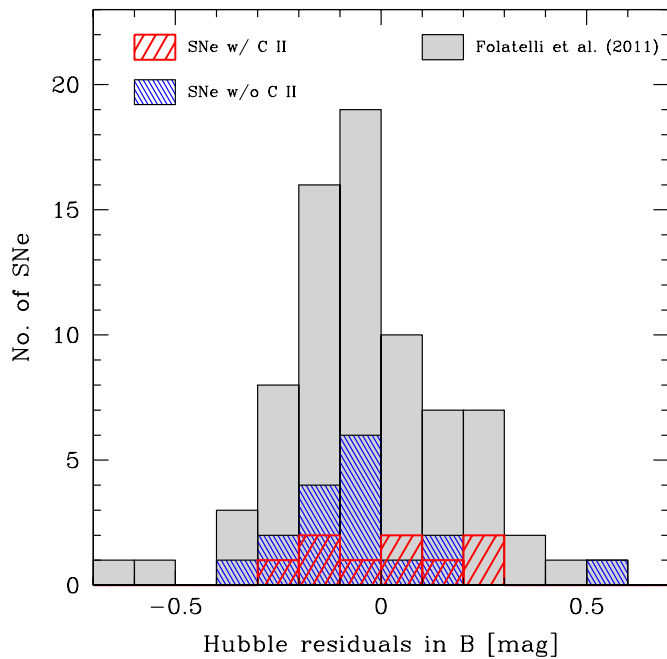


Figure 18. Distribution of B -band Hubble residuals based on Fit 2 of Table 8 in Folatelli et al. (2010). Shading code is the same as in Figure 15.

(A color version of this figure is available in the online journal.)

found evidence of $\text{C II } \lambda 6580$ absorption in at least 30% of the objects, which agrees closely with the findings of Parrent et al. (2011) based on a completely independent sample of publicly available spectra. The identification of this absorption with other elements, such as hydrogen, is considered unlikely (see Section 2.4). In addition, we have shown that nearly 10% of the SNe Ia in the CSP sample show a suppressed emission component of the $\text{Si II } \lambda 6355$ line, which SYNOW models indicate may be caused by absorption due to the same $\text{C II } \lambda 6580$ line. Taken together, these results imply that nearly half of all SNe Ia show carbon in their spectra at early phases, a finding

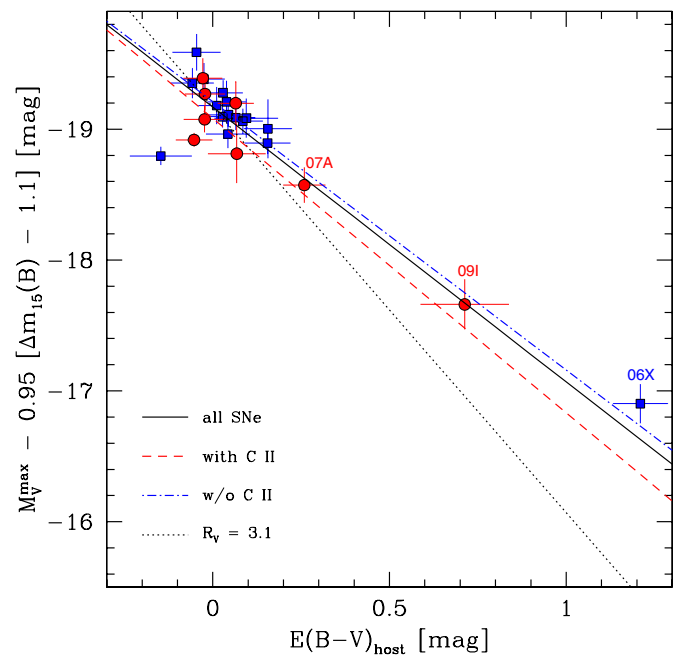


Figure 19. Decline-rate-corrected V -band absolute peak magnitude vs. $E(B - V)$ color excess for SNe Ia with (circles) and without (squares) carbon. The solid line is a straight-line fit to all the data points, while the dashed and dot-dashed lines correspond to the SNe Ia with and without carbon, respectively. As a reference, the dotted line corresponds to the case of $R_V = 3.1$. All three fits are in agreement with each other and favor a low value of R_V . Three SNe with the largest reddening—those which weigh most in the fits—are indicated.

(A color version of this figure is available in the online journal.)

that contradicts previous conclusions (e.g., see Thomas et al. 2007; Branch et al. 2007). The CSP spectra show clearly that the detection of C II absorption is a strong function of the age, falling from $>40\%$ at 10 days before B maximum to zero by the time of maximum itself. These results almost certainly represent a lower limit on the presence of unburned material in SNe Ia since very few events have been observed at even earlier phases.

Moreover, low signal-to-noise observations, or line blending when expansion velocities are high, also contribute to the difficulty of detecting the C II $\lambda 6580$ line. As we have shown, the latter effect can explain at least in part the absence of detectable carbon absorption in members of the HVG (Benetti et al. 2005) or BL (Branch et al. 2006) subclasses found by Parrent et al. (2011) and ourselves. As additional data are obtained at epochs of -10 days or earlier, it will be possible to corroborate whether, as we suspect, the majority of SNe Ia show carbon at some stage of their evolution. The theoretical implications of such findings are potentially large, in particular as pertains to the mechanism by which the explosive flame propagates inside the WD star.

The second remarkable finding from our study of the CSP spectra and the work of Parrent et al. (2011) is that assuming that the absorption observed at about 6300 \AA is due to C II $\lambda 6580$, then carbon must be present in very deep regions, corresponding to velocities as low as $v \approx 11,000 \text{ km s}^{-1}$, which is right above the bulk of silicon (Mazzali et al. 2007). This is well below the expected limit imposed by one-dimensional models and points directly to large mixing effects and/or possible departures from spherical symmetry or clumpiness.

In spherically symmetric models, irrespective of the details of the flame propagation (deflagration or detonation), the production of a large amount of ^{56}Ni as typically observed ($\sim 0.6 M_{\odot}$; see Stritzinger et al. 2006) requires that the strength of the flame—either its speed or the detonation transition density—is high, which must lead to the total consumption of carbon below $15,000 \text{ km s}^{-1}$ (e.g., Nomoto et al. 1984; Iwamoto et al. 1999), and even below $20,000 \text{ km s}^{-1}$ in detonation models (e.g., Shigeyama et al. 1992). The situation is different for non-spherical models. For example, the off-center ignition model of Maeda et al. (2010b; see also Kasen et al. 2009) synthesizes $0.54 M_{\odot}$ of ^{56}Ni , despite the relatively low density at which the detonation is triggered. The low transition density in their model results in less burning in the outer layers, and thereby the existence of carbon with a mass fraction of ~ 0.1 at velocities as low as $\sim 13,000 \text{ km s}^{-1}$. This is still larger than the observed velocity, but suggests that the non-spherical effects may be important in understanding the detection of carbon deep in the ejecta. This argument is based on the effect of a global asymmetry produced by the off-center ignition. Similar conclusions may be reached from possible effects of mixing or clump formation in multi-dimensional models.

The observed rate of carbon detections could thus provide information on the distribution of C-rich material, and the amount and size of the clumps. Unfortunately, the current uncertainties in the detection rate complicate these geometrical considerations. Nevertheless, if carbon were present in a single clump or asymmetric blob, the tight dispersion in expansion velocities of C II $\lambda 6580$ compared with silicon observed in Figure 13 would be surprising (see also Parrent et al. 2011).

In view of recent results which connect asymmetries in the ejecta with the observed spectroscopic and photometric diversity (Maund et al. 2010; Maeda et al. 2011), it is worth studying possible connections with the presence of unburned material in the ejecta. Breaking our sample of CSP SNe Ia into two groups depending on the presence or absence of HV components of Ca II absorption—a possible indicator of asymmetry (Tanaka et al. 2006)—we find no significant distinction in the frequency of detectable carbon. There is an indication in our data that SNe Ia with carbon show slightly bluer colors and lower luminosities at maximum light when compared with the rest of the sample. These are interesting hints of a possible origin of

the observed diversity arising from incomplete burning which may be related to the asymmetry scenario of Maeda et al. (2011), but the statistical significance of these results is limited by the sample size.

As shown in Section 2.3, modeling indicates that low masses of carbon in the range $M(\text{C}) \sim 10^{-3} - 10^{-2} M_{\odot}$ are enough to reproduce the observed spectral features, although HV components, undetectable due to blending with the Si II $\lambda 6355$ line, could increase this value by as much as an order of magnitude (Tanaka et al. 2011). Such small amounts of unburned material would make it difficult to detect other possible signatures in the observations. For instance, the non-detection of C I features in near-infrared spectra reported by Marion et al. (2006) could be explained by abundance and ionization state considerations (Tanaka et al. 2008).

Another interesting possibility is an enhancement of oxygen versus magnesium in SNe which suffered less complete burning. While oxygen may in part be primordial, magnesium is only a product of carbon burning. Determining the distribution of these elements in the outer ejecta may shed light on the evolution of the burning process (Mazzali et al. 2008). This could be attained with a temporal follow-up of the dominant spectral lines of these species, which at early times are those of O I and Mg II. Unfortunately, the study of such lines is complicated from an observational viewpoint. The main O I line at optical wavelengths usually coincides with the telluric A band, which makes it difficult to obtain an accurate measure of its strength from the ground. Other O I and Mg II lines appear blended with each other or with lines of other elements (e.g., see Figure 4). In this sense, the study of near-IR spectra may offer the possibility of finding isolated oxygen and magnesium lines (Marion et al. 2009).

Figure 11 clearly shows that the definitive assessment of the incidence of unburned material in SNe Ia requires a survey of early-time spectra—obtained at least 10 days before maximum light—covering the region of the C II lines. High signal-to-noise data are required in order to explore the possible presence of carbon in HV SNe Ia, in particular by observing the relatively unblended but weak C II $\lambda 7234$ line.

We are grateful to Wojtek Krzeminski for his dedicated efforts during the CSP campaigns. We also thank Luc Dessart for his useful suggestions, and Joseph Anderson, Francisco Förster, Giuliano Pignata, and the rest of the MCSS team for interesting discussions on the topic of this paper. This material is based upon work supported by NSF under grants AST-0306969, AST-0908886, AST-0607438, and AST-1008343. The Dark Cosmology Centre is funded by the Danish NSF. This research is supported by the World Premier International Research Center Initiative (WPI Initiative), MEXT, Japan. G.F. acknowledges financial support by Grant-in-Aid for Scientific Research for Young Scientists (23740175). M.H. acknowledges support by CONICYT through grants FONDECYT Regular 1060808, Centro de Astrofísica FONDAP 15010003, Centro BASAL CATA (PFB-06), and by the Millennium Center for Supernova Science (P06-045-F).

REFERENCES

- Altavilla, G., Stehle, M., Ruiz-Lapuente, P., et al. 2007, *A&A*, 475, 585
 Arnett, W. D., Truran, J. W., & Woosley, S. E. 1971, *ApJ*, 165, 87
 Benetti, S., Cappellaro, E., Mazzali, P. A., et al. 2005, *ApJ*, 623, 1011
 Branch, D., Benetti, S., Kasen, D., et al. 2002, *ApJ*, 566, 1005
 Branch, D., Dang, L. C., Hall, N., et al. 2006, *PASP*, 118, 560

- Branch, D., Garnavich, P., Matheson, T., et al. 2003, *AJ*, **126**, 1489
- Branch, D., Troxel, M. A., Jeffery, D. J., et al. 2007, *PASP*, **119**, 709
- Burns, C. R., Stritzinger, M., Phillips, M. M., et al. 2011, *AJ*, **141**, 19
- Contreras, C., Hamuy, M., Phillips, M. M., et al. 2010, *AJ*, **139**, 519
- Folatelli, G. 2010, in Proc. XXVIth IAP Annual Colloquium on Progenitors and Environments of Stellar Explosions (<http://www.iap.fr/col2010/Proceedings/posters/Folatelli.pdf>)
- Folatelli, G., Phillips, M. M., Burns, C. R., et al. 2010, *AJ*, **139**, 120
- Foley, R. J., & Kasen, D. 2011, *ApJ*, **729**, 55
- Gamezo, V. N., Khokhlov, A. M., & Oran, E. S. 2005, *ApJ*, **623**, 337
- Garavini, G., Folatelli, G., Goobar, A., et al. 2004, *AJ*, **128**, 387
- Hamuy, M., Folatelli, G., Morrell, N. I., et al. 2006, *PASP*, **118**, 2
- Hatano, K., Branch, D., Fisher, A., Millard, J., & Baron, E. 1999, *ApJS*, **121**, 233
- Hicken, M., Garnavich, P. M., Prieto, J. L., et al. 2007, *ApJ*, **669**, 17
- Hillebrandt, W., & Niemeyer, J. C. 2000, *ARA&A*, **38**, 191
- Höflich, P., & Khokhlov, A. M. 1996, *ApJ*, **457**, 500
- Höflich, P., Khokhlov, A. M., & Wheeler, J. C. 1995, *ApJ*, **444**, 831
- Höflich, P., Krisciunas, K., Khokhlov, A. M., et al. 2010, *ApJ*, **710**, 444
- Howell, D. A., Sullivan, M., Nugent, P. E., et al. 2006, *Nature*, **443**, 308
- Hoyle, F., & Fowler, W. A. 1960, *ApJ*, **132**, 565
- Iben, I., Jr., & Tutukov, A. V. 1984, *ApJS*, **54**, 335
- Iwamoto, K., Brachwitz, F., Nomoto, K., et al. 1999, *ApJS*, **125**, 439
- Kasen, D., Röpke, F. K., & Woosley, S. E. 2009, *Nature*, **460**, 869
- Kasen, D., & Woosley, S. E. 2007, *ApJ*, **656**, 661
- Khokhlov, A. M. 1991, *A&A*, **245**, 114
- Lentz, E. J., Baron, E., Hauschildt, P. H., & Branch, D. 2002, *ApJ*, **580**, 374
- Lucy, L. B. 1999, *A&A*, **345**, 211
- Maeda, K., Benetti, S., Stritzinger, M., et al. 2010a, *Nature*, **466**, 82
- Maeda, K., Leloudas, G., Taubenberger, S., et al. 2011, *MNRAS*, **413**, 3075
- Maeda, K., Röpke, F. K., Fink, M., et al. 2010b, *ApJ*, **712**, 624
- Marietta, E., Burrows, A., & Fryxell, B. 2000, *ApJS*, **128**, 615
- Marion, G. H., Höflich, P., Gerardy, C. L., et al. 2009, *AJ*, **138**, 727
- Marion, G. H., Höflich, P., Wheeler, J. C., et al. 2006, *ApJ*, **645**, 1392
- Maund, J. R., Höflich, P., Patat, F., et al. 2010, *ApJ*, **725**, 167
- Mazzali, P. A. 2000, *A&A*, **363**, 705
- Mazzali, P. A. 2001, *MNRAS*, **321**, 341
- Mazzali, P. A., Benetti, S., Altavilla, G., et al. 2005, *ApJ*, **623**, 37
- Mazzali, P. A., & Lucy, L. B. 1993, *A&A*, **279**, 447
- Mazzali, P. A., Röpke, F. K., Benetti, S., & Hillebrandt, W. 2007, *Science*, **315**, 825
- Mazzali, P. A., Sauer, D. N., Pastorello, A., Benetti, S., & Hillebrandt, W. 2008, *MNRAS*, **386**, 1897
- Nomoto, K. 1982, *ApJ*, **253**, 798
- Nomoto, K., Saio, H., Kato, M., & Hachisu, I. 2007, *ApJ*, **663**, 1269
- Nomoto, K., Sugimoto, D., & Neo, S. 1976, *Ap&SS*, **39**, L37
- Nomoto, K., Thielemann, F.-K., & Yokoi, K. 1984, *ApJ*, **286**, 644
- Nugent, P., Phillips, M., Baron, E., Branch, D., & Hauschildt, P. 1995, *ApJ*, **455**, 147
- Pakmor, R., Röpke, F. K., Weiss, A., & Hillebrandt, W. 2008, *A&A*, **489**, 943
- Parrent, J. T., Thomas, R. C., Fesen, R. A., et al. 2011, *ApJ*, **732**, 30
- Pastorello, A., Mazzali, P. A., Pignata, G., et al. 2007, *MNRAS*, **377**, 1531
- Perlmutter, S., Aldering, G., Goldhaber, G., et al. 1999, *ApJ*, **517**, 565
- Phillips, M. M. 1993, *ApJ*, **413**, 105
- Pignata, G., Benetti, S., Mazzali, P. A., et al. 2008, *MNRAS*, **388**, 971
- Pinto, P. A., & Eastman, R. G. 2000, *ApJ*, **530**, 757
- Riess, A. G., Filippenko, A. V., Challis, P., et al. 1998, *AJ*, **116**, 1009
- Röpke, F. K. 2005, *A&A*, **432**, 969
- Scalzo, R. A., Aldering, G., Antilogus, P., et al. 2010, *ApJ*, **713**, 1073
- Shigeyama, T., Nomoto, K., Yamaoka, H., & Thielemann, F.-K. 1992, *ApJ*, **386**, 13
- Silverman, J. M., Ganeshalingam, M., Li, W., et al. 2011, *MNRAS*, **410**, 585
- Stanishev, V., Goobar, A., Benetti, S., et al. 2007, *A&A*, **469**, 645
- Stritzinger, M., Burns, C. R., Phillips, M. M., et al. 2010, *AJ*, **140**, 2036
- Stritzinger, M., Mazzali, P. A., Sollerman, J., & Benetti, S. 2006, *A&A*, **460**, 793
- Stritzinger, M., Phillips, M. M., Boldt, S. L., et al. 2011, *AJ*, **142**, 156
- Tanaka, M., Kawabata, K. S., Yamanaka, M., et al. 2010, *ApJ*, **714**, 1209
- Tanaka, M., Mazzali, P. A., Benetti, S., et al. 2008, *ApJ*, **677**, 448
- Tanaka, M., Mazzali, P. A., Maeda, K., & Nomoto, K. 2006, *ApJ*, **645**, 470
- Tanaka, M., Mazzali, P. A., Stanishev, V., et al. 2011, *MNRAS*, **410**, 1725
- Taubenberger, S., Benetti, S., Childress, M., et al. 2011, *MNRAS*, **412**, 2735
- Taubenberger, S., Hachinger, S., Pignata, G., et al. 2008, *MNRAS*, **385**, 75
- Thomas, R. C., Aldering, G., Antilogus, P., et al. 2007, *ApJ*, **654**, 53
- Wang, X., Filippenko, A. V., Ganeshalingam, M., et al. 2009, *ApJ*, **699**, 139
- Webbink, R. F. 1984, *ApJ*, **277**, 355
- Whelan, J., & Iben, I., Jr. 1973, *ApJ*, **186**, 1007
- Yamanaka, M., Kawabata, K. S., Kinugasa, K., et al. 2009a, *ApJ*, **707**, 118
- Yamanaka, M., Naito, H., Kinugasa, K., et al. 2009b, *PASJ*, **61**, 713